University of Szeged

Faculty of Pharmacy

Department of Medical Chemistry

INTRACELLULAR PROTEIN DELIVERY WITH THE USE OF ENDOCYTOSIS ROUTING SEQUENCES

Ph. D. Thesis

Norbert Imre

Supervisor:

Prof. Dr. Martinek Tamás

2020

Table of contents

List of publications and lectures iv

Abbreviations vi

1. Introduction and aims 1

2. Literature background 3

2.1. The eukaryotic cell membrane 3

2.1.1. Structure of the membrane 3

2.1.2. Transport across the membrane 4

2.2. Gangliosides 7

2.2.1. Structure of gangliosides 7

2.3. Intracellular delivery 9

2.3.1. Therapeutic use and challenges 9

2.3.2. Intracellular delivery of peptides and proteins 11

2.3.3. Intracellular delivery of antibodies 12

2.3.4. Internalization through gangliosides 13

3. Experimental methods 14

3.1. Synthesis and purification of peptides 14

3.2. Isothermal titration calorimetry 14

3.3. NMR experiments 15

3.4. Tryptophan fluorescence blue-shift measurements 15

3.5. Circular dichroism 16

3.6. Cell cultures 16

3.7. Preparation of the carrier–protein complexes 16

3.8. Flow cytometry 16

3.9. Live confocal laser scanning microscopy 17
3.10. Image analysis 18
3.11. Cytotoxicity assay 19
3.12. Statistical analysis 19
4. Results and discussion 20
4.1. Biophysical characterization of the WYKYW–GM1 binding 20
4.1.1. High affinity and specificity 21
4.1.2. Structural requirements of the binding 23
4.1.3. The role of membrane components 26
4.2. Endocytosis-inducing properties of the WYKYW tag 28
4.2.1. Lipid raft-mediated endocytosis 28
4.2.2. A single WYKYW copy is enough to induce endocytosis 32
4.2.3. Intracellular delivery of an antibody complex 34
4.2.4. Functionality of the delivered cargoes 37
5. Conclusions 43
6. Summary 45
7. Acknowledgements 47
8. References 48

List of publications and lectures

Full paper and patent related to the thesis

I. N. Imre, A. Hetényi, E. Szabó, B. Bodnár, A. Szkalisity, I. Gróf, A. Bocsik, M. A. Deli, P. Horvath, Á. Czibula, É. Monostori, T. A. Martinek (**2020**). Routing Nanomolar Protein Cargoes to Lipid Raft-Mediated/Caveolar Endocytosis through a Ganglioside GM1-Specific Recognition Tag. *Advanced Science*, 7, 1902621

IF (2019): 15.84

II. N. Imre, A. Hetényi, E. Szabó, B. Bodnár, A. Szkalisity, I. Gróf, A. Bocsik, M. A. Deli, P. Horvath, Á. Czibula, É. Monostori, T. A. Martinek. ENDOCYTOSIS ROUTING SEQUENCE PEPTIDE FOR CELL DELIVERY SYSTEMS, Patent Application, Patent Number: P1900205, IP share: 20%

Other full papers

I. R. Ismail, T. Sovány, A. Gácsi, R. Ambrus, G. Katona, N. Imre, I. Csóka (**2019**). Synthesis and Statistical Optimization of Poly (Lactic-Co-Glycolic Acid) Nanoparticles Encapsulating GLP1 Analog Designed for Oral Delivery *Pharmaceutical Research, 36,* 99

IF: 3.242

II. A. Bocsik, I. Gróf, L. Kiss, F. Ötvös, O. Zsíros, L. Daruka, L. Fülöp, M. Vastag, Á. Kittel, N. Imre, T. A. Martinek, C. Pál, P. Szabó-Révész, M. A. Deli (**2019**). Dual Action of the PN159/KLAL/MAP Peptide: Increase of Drug Penetration across Caco-2 Intestinal Barrier Model by Modulation of Tight Junctions and Plasma Membrane Permeability. *Pharmaceutics, 11*, 73.

IF: 4.421

III. Zs. Hegedüs, I. Makra, N. Imre, A. Hetényi, I. M. Mándity, É. Monostori, T. A. Martinek (**2016**). Foldameric probes for membrane interactions by induced β-sheet folding. *Chemical Communications, 52*, 1891

IF: 6.319

Scientific lectures related to the thesis

1. N. Imre, A. Hetényi, E. Szabó, B. Bodnár, A. Szkalisity, I. Gróf, A. Bocsik, M. A. Deli, P. Horvath, Á. Czibula, É. Monostori, T. A. Martinek

   IgG bejuttatása specifikus GM1 gangliozid felismerő szekvenciával

   MTA Gyógyszerkémiai és Gyógyszertechnológiai Szimpózium

   Kecskemét, 2019. szeptember 5-6.

2. N. Imre, A. Hetényi, E. Szabó, B. Bodnár, A. Szkalisity, I. Gróf, A. Bocsik, M. A. Deli, P. Horvath, Á. Czibula, É. Monostori, T. A. Martinek

   IgG bejuttatása specifikus GM1 gangliozid felismerő szekvenciával

   MTA Peptidkémiai Munkabizottság Tudományos Ülése

   Balatonszemes, 2019. május 27-29.

3. N. Imre, B. Bodnár, E. Szabó, É. Monostori, T. A. Martinek

   Gangliozid-mediált sejtpenetráció

   MTA Peptidkémiai Munkabizottság Tudományos Ülése

   Balatonszemes, 2018. május 28-30.

Abbreviations

AP-2: adaptor protein complex 2

ATP: adenosine triphosphate

CD: circular dichroism

CFU: 5(6)-carboxyfluorescein

CLIC: clathrin- and dynamin-independent carrier

CLSM: confocal laser scanning microscopy

CPP: cell-penetrating peptide

CTX-B: choleratoxin B subunit

DBU: 1,8-diazabicycloundec-7-ene

DCM: dichloromethane

DIEA: diisopropylethylamine

DMF: *N*,*N*-dimethylformamide

DPC: *n*-dodecylphosphocholine

ESI-MS: electrospray ionization mass spectrometry

FACS: fluorescence activated cell sorting

FITC: fluorescein isothiocyanate

GEEC: glycosyl phosphatidylinositol-anchored protein enriched early endosomal compartment

GFP: green fluorescent protein

HATU: 1-[bis(dimethylamino)methylene]-1*H*-1,2,3-triazolo[4,5-*b*]-pyridinium-3-oxide hexafluorophosphate

HIV-1: human immunodeficiency virus 1

ITC: isothermal titration calorimetry

LDL: low density lipoprotein

MEM: modified Eagle’s medium

NA: NeutrAvidin

NMR: nuclear magnetic resonance

PBS: phosphate buffered saline

PPI: protein–protein interaction

PTD: protein transduction domain

RPE: r-phycoerythrin

RP-HPLC: reverse phase high pressure liquid chromatography

RPMI: Roswell Park Memorial Institute buffer

STD: saturation transfer difference

SV40: simian virus 40

TAT: trans-activator of transcription

TFA: trifluoroacetic acid

1. Introduction and aims

One of the greatest challenges to overcome in drug development is the efficient translocation of protein-sized drugs into cells, because the mammalian cell membrane acts as a major obstacle to these hydrophilic large molecules, which could otherwise be highly specific, efficient, and tolerable pharmaceuticals[1, 2]. Internalization of these molecules can be achieved by clathrin-independent endocytosis (such as lipid-raft mediated/caveolar endocytosis[3, 4]), and this pathway is exploited by endogenous proteins[5], bacterial toxins (cholera and tetanus)[6], and viruses (murine polyomavirus[7] and echovirus 1[8]), because this pathway tends to fuse with lysosomes only after a very long endosomal retention time, if at all. This endocytic mechanism is an attractive target to deliver functional proteins without degradation, and the leaky endosomes forming in the process allow direct escape for the molecules before moving to other cellular locations[8]. The surface of these lipid rafts and caveolar pits are composed of various glycosphingolipids, especially of mono-, di-, and trisialotetrahexosylgangliosides (GM1, GD1a, GT1b), which are the major receptors for the natural cargoes. Binding and clustering the gangliosides induce an endocytic mechanism, where lysosomal fusion is negligible[9], allowing the proteins to reach the cytosol or undergo transcytosis[10-13]. Many delivery systems fail to avoid lysosomal entrapment, or the molecule responsible for the internalization is required to be used at therapeutically irrelevant, high concentrations[14]. Interpreting the glycan code by studying how gangliosides trigger endocytosis could be the key to solve these problems. Interest in binding gangliosides has already arisen; however, high-affinity molecular recognition is still a great challenge[15]. The specific targeting of ganglioside GM1 is especially sought, because this ganglioside, while normally being expressed in many mammalian cell types, is highly abundant in cancerous cells[16, 17]. Therapeutic protein levels in the extracellular fluid yield 100–500 nM[18]; therefore, a high-affinity interaction is needed to create a cell membrane enrichment that facilitates sufficient material flux in clinical applications.

Our main goal was to achieve nanomolar delivery of large proteins (up to the size of antibodies) via lipid raft-mediated endocytosis. We aimed to use a non-toxic peptide tag to mimic the ganglioside-mediated internalization of endogenous and exogenous proteins; therefore, we set out to find a minimal motif that can bind ganglioside GM1 with high affinity and specificity. By focusing on a structurally well-defined receptor and conducting a thorough biophysical

characterization of the interaction, we aimed to open a way to structure-based design, which is rare in protein delivery approaches. We set out to investigate the ability of the characterized peptidic tag to deliver large proteins into the cells, while rigorously monitoring its toxicity, mechanism of entry, and the tendency to fuse with lysosomes. Using a medicinal chemistry approach, we set out to establish a structure–activity relationship, to gain insight into the binding mechanism, and to improve the enzymatic stability while retaining high affinity.

2. Literature background

2.1. The eukaryotic cell membrane

2.1.1. Structure of the membrane

Life can be defined as myriads of biochemical reactions continuously taking place in a synchronized way. What brings order to the (at first glance) chaos is that these reactions are separated by both time and space. This is achieved by biological barriers around the cells and the organelles: the membranes. Eukaryotic membranes are formed by an oriented double layer of molecules (mostly phospholipids), having a hydrophobic core with polar moieties facing the aqueous solutions. Biochemical reactions only occurring in aqueous media is a false notion: the inner core of the membrane is in a condensed state, and crucial processes take place within it with the aid of the countless membrane-bound proteins. Our current understanding of the structure of the membranes is built on the "fluid mosaic" model of Singer and Nicolson (Figure 1)[19].

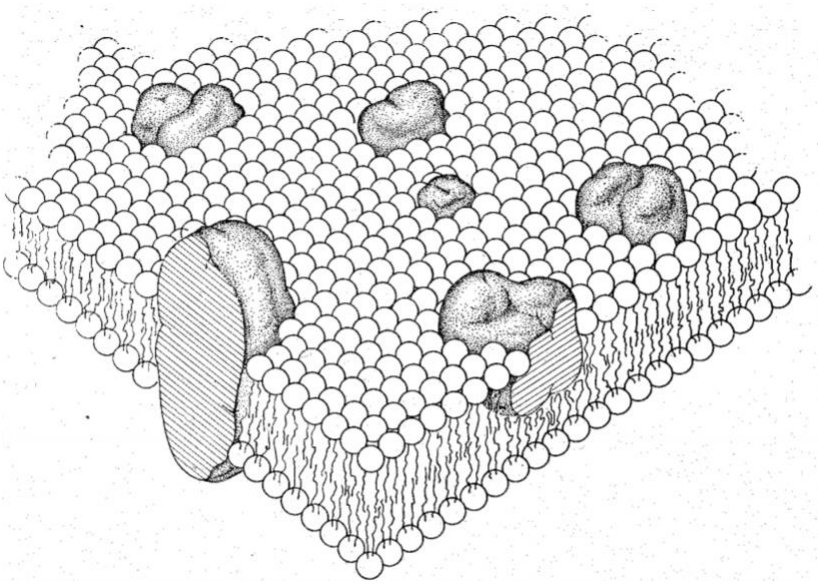

Figure 1. The original "fluid mosaic" membrane model of Singer–Nicolson.

Amphipathic molecules, such as sterols, glycolipids, and phospholipids are the most abundant building blocks of the membrane, and these can self-organize in the aqueous media, creating a bilayer, in which the hydrophobic parts are facing each other[20]. Membrane proteins can be found near the polar headgroups or be associated with the hydrophobic core[21]. The "fluid" refers to the constant motion of proteins and lipids alike. Both classes have rotational motion and translational diffusion, which is necessary for their functionality[22]. The membrane is asymmetrical,

arises from the lack of transbilayer (flip-flop) motion of the membrane proteins. While all membrane building lipids can be found on both sides of the membrane, their distribution is different for the intra- and extracellular leaflets, and certain proteins are quite often anchored to only one side of the bilayer[23]. Although many years have passed since the Singer–Nicolson model emerged, and it is still considered to be the best model available, extensive research of the field revealed several refinements to be made. The original model depicted transmembrane proteins as scarce; however, according to the current view, most of the bilayer is perturbed by these proteins[24-26]. These perturbations cause the curving of membranes, which can be very significant in secretion vesicles or near a fission event requiring specific proteins such as dynamin or clathrin[27, 28]. The ever dynamic curving of membranes is found to be an important factor in regulating enzymes, cell growth, and movement[29, 30]. Shape changes arising from the plasma membrane tension regulate the generation of the caveolae- and clathrin-mediated endocytosis[31]. Another important emerging feature of the enhanced membrane model is that there exists a lateral heterogeneity amongst both proteins and lipids. These domains arise, because membrane lipids are not fully intermiscible[32], and several proteins were shown to block translational diffusion because of the anchoring effects of protein–protein interactions (PPIs)[33]. An important species of these domains is the membrane raft. Membrane rafts are small, heterogeneous, highly dynamic sphingolipid- and sterol-enriched patches, with important signaling functions[34, 35].

2.1.2. Transport across the membrane

It is essential for cell functions that certain molecules can cross the membrane bilayer in a controlled manner. The mechanism of internalization (and externalization) differs for the classes of chemical substances. Low-molecular-weight and moderately polar molecules obeying Lipinski's rule of five[36] can diffuse passively across the membrane. This mechanism is only driven by the electric and concentration gradient; therefore, it is energy independent[37]. The mammalian membrane is impermeable to larger, polar molecules, and charged chemical entities, such as ions[38]. To facilitate the entry of these species, cell membrane transporters are utilized. Passive transporters allow diffusion without the use of energy, unlike active transporters, which can work against the concentration gradient. Ions can either be actively transported by ion pumps, or they can passively travel through ion channels with high selectivity[39]. Ionophore molecules, which can shuttle ions, are of emerging importance in the combat against microbes and various diseases as well[40, 41]. Small molecules, including water are often transported[42]. Nucleobases, sugars, amino acids, and even

small peptides have their specific transporters for their entry or export[43-45]. An important subclass of membrane transport is the vesicular transport (Figure 2)[46]. These processes are energy dependent, as they require ATP; therefore, in contrast to the passive transport mechanisms, they are inhibited at a reduced temperature[47].

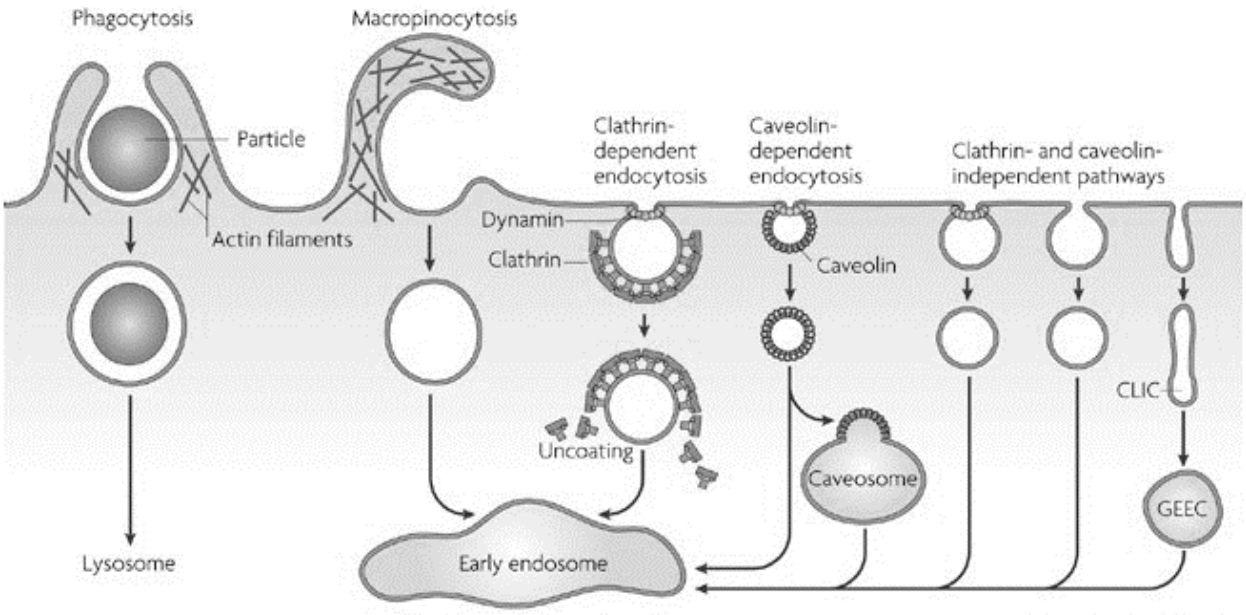

Figure 2. Types of vesicular transport mechanisms. CLIC: clathrin- and dynamin-independent carrier; GEEC: glycosyl phosphatidylinositol-anchored protein enriched early endosomal compartment.

We can further classify them by their direction (endo- and exocytosis), or their specificity: phagocytosis engulfs specific solid matters to break them down, while pinocytosis aids the transport of already dissolved cargoes[48]. Pinocytosis can be divided into different classes. One of the most studied is clathrin-dependent receptor-mediated endocytosis, in which ligands (for example, transferrin, antibodies, LDL) are being transferred to the cytoplasm in clathrin-coated vesicles, budding from a clathrin and AP-2 protein-enriched pit[49, 50]. Upon addition of chlorpromazine to mammalian cells, the receptors disappear and the pathway gets blocked, which makes chlorpromazine a useful tool in studying endocytic mechanisms[51]. Macropinosomes are relatively huge (up to a hundred of coated vesicles), and they provide an efficient way for macromolecules to internalize[52]. They play an important part in the immune response, helping cells to capture a broad range of antigens[53]. This lack of specificity is exploited by various

pathogens, such as prions and prion-like proteins[54], or the Ebolavirus[55]. Inhibiting this pathway can be accomplished by specifically blocking phosphoinositide 3-kinase with wortmannin[56], but many new inhibitor molecules are under excessive research, as macropinocytosis was shown to help tumor drug resistance[57]. As previously mentioned, certain invaginations of the membrane called the lipid rafts are enriched in cholesterol and glycosphingolipids (Figure 3)[58].

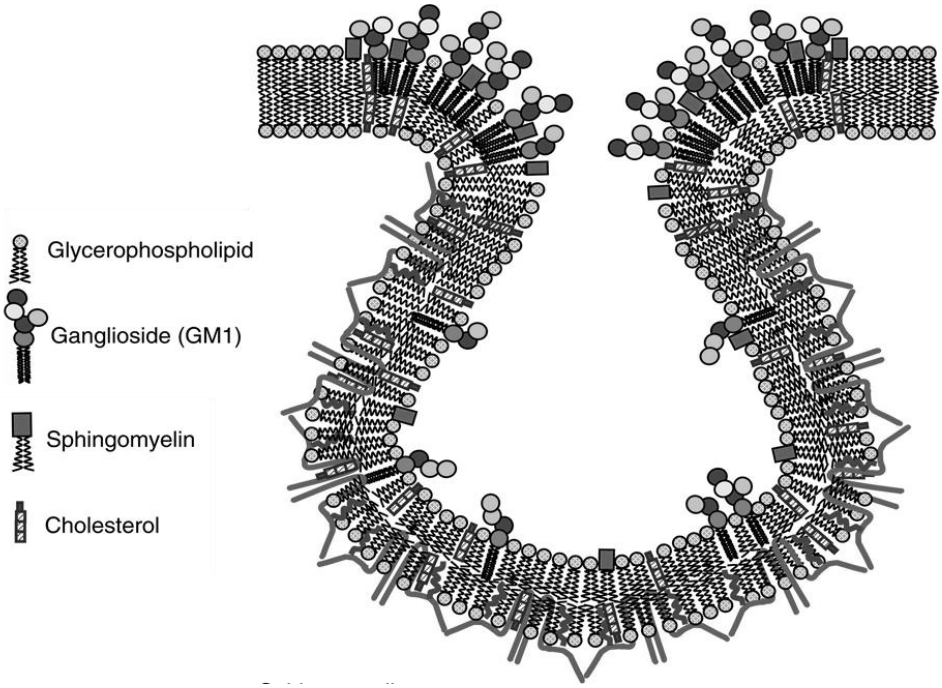

Figure 3. A representation of a membrane raft.

These microdomains in the membrane are highly transient[59], and internalization of ligands through this mechanism is called lipid raft-mediated endocytosis. Caveolae form a subspecies of lipid rafts, which are formed by the caveolin-1 protein[60]. Caveolar and noncaveolar endocytosis of the lipid rafts can be either dynamin dependent, or independent; however, a common feature of them is that they show clathrin-independence, and high cholesterol sensitivity. Depleting cholesterol with methyl-β-cyclodextrin, filipin or nystatin can inhibit the expressions of caveolae and the lipid raft-mediated endocytosis[61-63]. Lipid rafts are important platforms for cell-signaling as numerous signaling molecules were found to be localized in these smooth invaginations[64, 65]. Lipid characterization identified the enrichment of various glycosphingolipids in these domains, namely, gangliosides GM1, GM3, GD3, and GD1a[66, 67]. These molecules are utilized for entry into the cells by the SV40 virus, and the toxins of bacteria Shiga and Cholera[68, 69].

2.2. Gangliosides

2.2.1. Structure of gangliosides

Biomolecules consisting of a carbohydrate chain linked to a lipid part through glycosidic linkage are the glycolipids. If the lipid moiety is a sphingosine or a ceramide, they are classified as glycosphingolipids. Sialic acid-containing glycosphingolipids, which are mainly found in the nervous system, were named 'gangliosides' by Ernst Klenk[70]. The class shows a very high diversity (more than 150 derivatives have been identified) deriving from both the variety of the carbohydrate moiety and the heterogeneity of the lipophilic part[71].

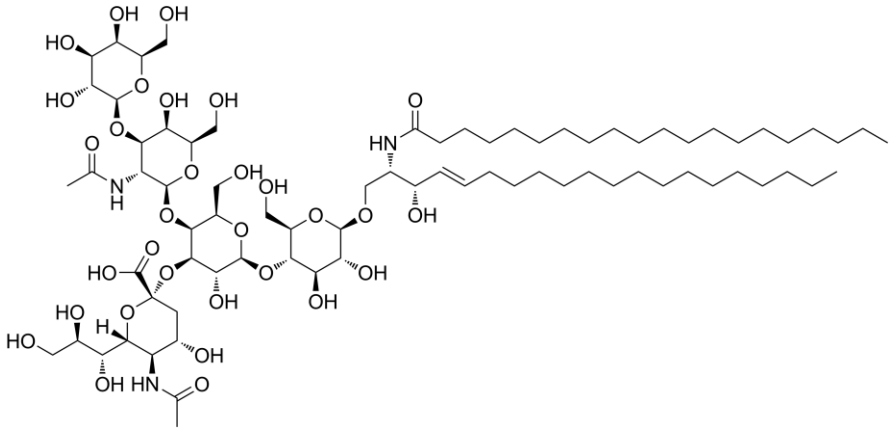

Figure 4. Structure of ganglioside GM1 [Galβ1-3GalNAcβ1-4(Neu5Acα2-3)Galβ1-4GlcβCer]. The lipophilic part contains a sphingosine and a stearic acid, which are linked to a β-D-glucose. The carbohydrate chain continues as follows: β-D-galactose, *N*-acetyl-β-D-galactosamine, β-D-galactose, with sialic acid (*N*-acetyl-α-neuraminic acid) branching off the inner β-D-galactose.

The nomenclature of sugars is too complex for everyday use; hence, Lars Svennerholm invented a terminology to easily identify and refer to gangliosides[72]. In this naming convention, G refers to the ganglioside series, the second letter refers to the number of sialic acids (mono, di, tri), and the last number refers to the order of migration on a thin-layer chromatogram. The glycosphingolipids can have 0–3 sialic acid moieties linked to the inner galactose residue, which gives rise to the asialo-, a-, b-, and c-series, respectively. Human gangliosides mostly utilize *N*-acetylneuraminic acid as a sialic acid derivative, while in many other mammals *N*-glycolylneuraminic acid can be also found[73]. Gangliosides are synthesized from lactosylceramide in the endoplasmic reticulum and later modified in the Golgi apparatus[74]. The reactions are

catalyzed in a committed way by specific glycosyltransferases, which can compete for the same precursor (Figure 5).

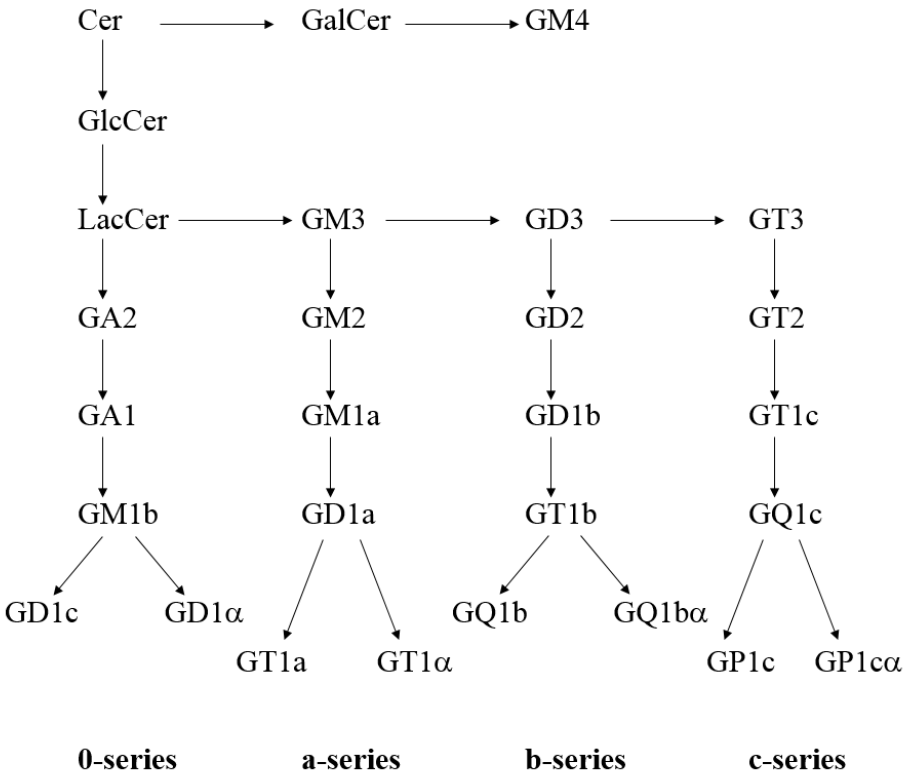

Figure 5. Biosynthetic pathways of gangliosides. Cer: ceramide, GalCer: galactosylceramide, GlcCer: glucosylceramide, LacCer: lactosylceramide.

Although all cells synthesize gangliosides, their forms vary with the expression of level of these enzymes[75]. It is worth to note, that certain gangliosides are overexpressed in various cancers, making them a desirable target in antitumor therapies[76, 77].

Gangliosides are linked to many diseases, for example, lysosomal storage disfunctions (Tay-Sachs and Sandhoff diseases), Guillan–Barré syndrome, and they seem to be involved in type 2 diabetes[78, 79]. The most common neurodegenerative disorder, the Alzheimer's disease is initiated by the aggregation of amyloid-β peptides, which is thought to be caused by gangliosides[80]. It has been suggested, that gangliosides can modulate angiogenesis, which supports tumor growth in both ways[81]. Gangliosides also serve as receptors for various pathogens. Influenza virus A recognizes sialic acid residues to invade host cells[82]. As previously mentioned, simian virus 40 (SV40) and the choleratoxin B subunit (CTX-B) specifically bind to GM1 ganglioside[68, 83]. It was well

established that the pentameric protein subunit of the choleratoxin crosslinks 5 ganglioside molecules results in endocytosis[84]. However, it was recently suggested that a single-point binding is sufficient for the internalization and intoxication[85]. A very similar entry method is utilized by the Escherichia coli heat-labile enterotoxin and the Shiga toxin[86]. Tetanus and botulinum toxins also bind to b-series gangliosides[87, 88].

2.3. Intracellular delivery

2.3.1. Therapeutic use and challenges

Several active pharmaceutical ingredients, especially large, polar molecules (such as proteins, antibodies, DNA) need to reach the intracellular compartment to exert their therapeutic effect. Small-molecule drugs readily cross the biological membranes. However, they cannot generally modulate protein–protein interactions, which regulate essential cell functions and take part in the signaling pathways of cancer pathogenesis.[89] These interactions involve large 2000–3000 $Å^2$ surfaces compared to the small-molecule–protein interactions of 500–1000 $Å^2$ [90]. Approved drugs can access less than 700 proteins, which is smaller compared to the amount of targetable proteins[91, 92].

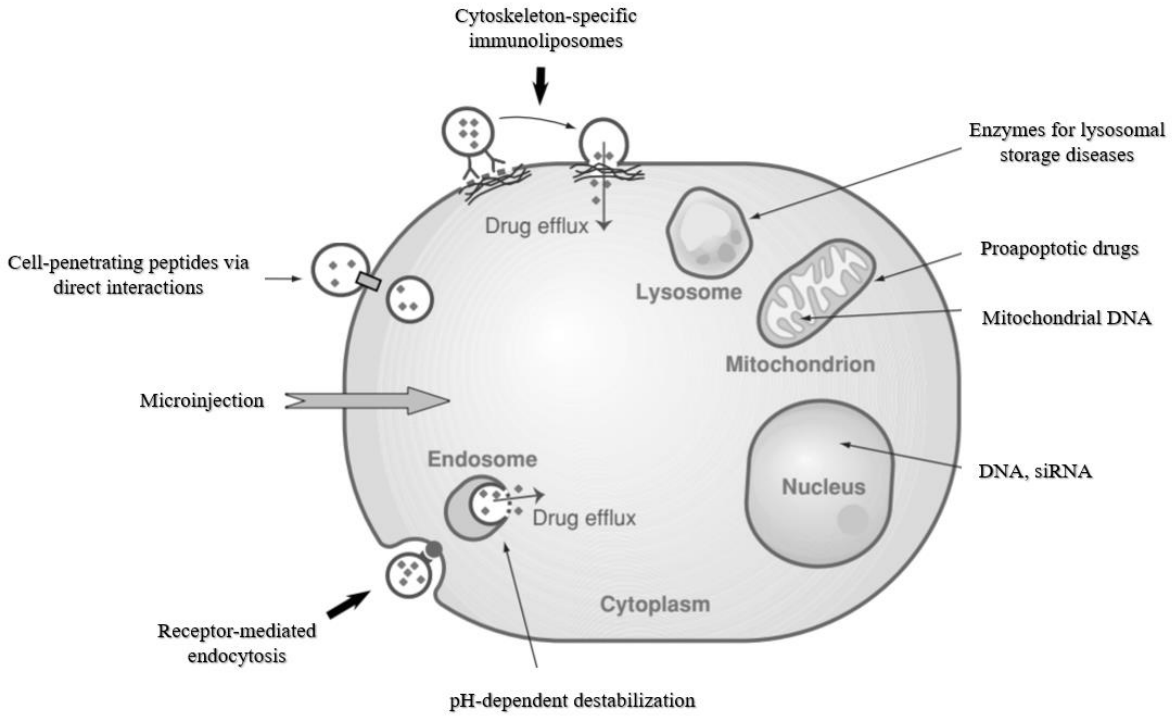

Figure 6. A simplified representation of intracellular targets and methods of delivery.

Multiple attempts have been made (Figure 6), but only partial successes were achieved, because of the difficult challenges in this area. Physical methods, like electroporation or microinjection are invasive methods and, therefore, can alter the membrane[93, 94]. Most cell delivery methods are non-specific to different cells; however, selective cell and tissue targeting is a quickly emerging hot topic[95]. One of the most important problems is, that even if a cargo gets through the membrane, it gets trapped in endosomes, and then it may end up in lysosomes resulting in degradation[96]. To overcome this, the use of pH-sensitive liposomes and pH-responsive cell-penetrating peptides was developed. These destabilize the endosomal membrane when being activated by the decreasing pH[97]. Naturally, reaching the cytosol is rarely sufficient: active pharmaceutical ingredients have to find their way to the specific organelles, such as nuclei or mitochondria, where they can exert their effect. Reaching the nuclei is especially sought in the case of gene therapy, which is considered to be the most advanced treatment in various diseases[98, 99]. Using viral vectors for the delivery of DNA has risks of viral complications, while non-viral delivery systems such as cationic lipids and cationic liposomes lack specificity and are severely cytotoxic[100].

Cell-penetrating peptides (CPPs) or protein transduction domains (PTDs), which are short, mostly cationic or amphiphilic peptides that can inherently cross the membrane have been in the focus of cell delivery in the last 20–30 years. Ever since the discovery of their archetypes, the *trans*-activating transcriptional activator (TAT)[101, 102] from HIV-1 and the peptide derived from the third helix of the *Drosophila Antennapedia* homeodomain (penetratin)[103], countless candidates have been synthesized, including elegant cyclic[104, 105], stapled[106], and foldamer[107] derivatives. Cell-penetrating peptides, however, have not lived up to the expectations so far, because the extracellular concentration needed to exert their effects are often in the micromolar range, where certain toxic side effects can occur[108, 109]. Moreover, even though hundreds of sequences have been identified and synthesized, in most cases, they are only capable of internalizing alone or with a small molecular fluorescent dye. Only 4% of them can deliver macromolecules such as proteins into the cells, which could specifically and selectively alter PPIs[110].

2.3.2. Intracellular delivery of peptides and proteins

The most studied protein delivery into the mammalian cells is the CPP-mediated restoration of p53 protein function. Most human tumors lack p53 gene activity, which suppresses tumor growth and restoring its function can inhibit the growth and proliferation of the cancer cells. Fusing the N-terminal of the p53 protein with TAT peptide yielded increased accumulation of the cargo in cells and decreased binding by its negative regulator (HDM2), resulting in increased killing of tumor cells[111]. Fusing the C-terminal of the protein to TAT in a similar approach was shown to be effective *in vivo*[112]. Various tumor suppressor peptides (P16, VHL) and proteins (p27) were conjugated with TAT or penetratin peptides, which reduced cell proliferation of cancer cells. However, normal cells were affected by the treatment too, which raises concerns about the selectivity[113–115]. Facilitation of antitumor effects was achieved with several cell-penetrating peptides linked to apoptosis regulatory proteins such as Bcl-2 family proteins, S100 family proteins, activating transcription factor 2, and smac peptide[116–118].

There is another emerging subclass of internalizing molecules, the supercharged proteins. They are engineered or naturally occurring proteins with unusually high net theoretical charge (>1 net charge unit per kDa). It has been suggested that engineered, highly positively charged GFP variants can penetrate cells and deliver other macromolecules.[119] Similar naturally occurring human proteins have the ability to deliver functional cargo both *in vitro* and *in vivo*.[120] The

internalization mechanism of these proteins is yet unclear, and supercharging molecules may alter their properties and activity.

2.3.3. Intracellular delivery of antibodies

The antibody–antigen interaction is the most specific molecular recognition event occurring in nature. Pharmaceutical companies, consequently, are more and more focused on antibody-based therapies, the delivery of functional, intact antibodies (155 kDa molecular weight), and protein complexes are ~~is~~ highly sought after. Apart from a small fraction of naturally occurring autoantibodies, which appear in autoimmune diseases[121, 122], their size and hydrophilicity make them unable to cross biological membranes. Strategies that evolved to overcome this barrier can be classified in 4 major classes: direct physical methods, intracellular expression, fusion with intrinsically internalizing autoantibody moieties or protein-transduction domains, and delivery with nanoparticles. As previously mentioned, direct delivery methods (microinjection, electroporation) have *in vivo* safety and efficiency issues, while lacking cell specificity. Nevertheless, these methods allow direct delivery into the cytosol, with the ability of targeting intracytoplasmical structures, when using localization signals on the cargo[123]. The intrabody technique can be achieved by cell transfection with viruses or plasmids, which carry the gene encoding the antibody. Advantages of this method include the ease of directing the intrabody to specific cell compartments. In contrast, an efficient, safe, and tissue-specific DNA transfection method is still sought after. Translating this method into clinical studies also requires addressing the delayed onset of the effect, and the normalization of the duration and level of expression. Extensive research of the field, however, led to a few successful candidates, which have been clinically approved[124, 125]. Internalization with nanocarriers can deliver a high amount of payload, while protecting the cargo from serum enzymes[126]. With the tunable composition and the availability of decoration of the carrier system, cell-targeting and sustained release can be achieved[127–129]. Their disadvantages include the cargo being trapped in endosomes, immunogenicity caused by the relatively large size, and tedious and expensive production.

Fusing the cargo with a part of inherently internalizing autoantibodies or their moieties, or protein-transduction domains and their mimics is a field under extensive research[130–132]. In the simplest case, using only natural amino acids and naturally occurring carrier sequences can be expressed together with the cargo antibodies. However, with the rise of foldameric, stapled,

cyclized derivatives and the benefits of using modular chemistry, chemical synthesis is more often used. This enables the quick re-engineering of sequences but introduces an often-challenging linker chemistry. A possible disadvantage compared to the previous methods is that direct covalent link to the cargo antibodies can alter their potency and selectivity. Cell- and tissue-specificity is usually not sufficient without the use of specific cell-homing peptides, and the endosomal entrapment is a serious disadvantage of CPPs too. Endosomolytic, pH-activating cell-penetrating sequences are under extensive research with a few very successful adaptations[133, 134]. The effective extracellular concentration used in these methods, however, can limit the translation of these methods towards *in vivo* clinical trials, and research groups must focus on finding cell delivery methods which can be used in the low-nanomolar range.

2.3.4. Internalization through gangliosides

A subset of protein toxins utilizes gangliosides as host receptors due to their extracellular localization and essential nature in host phsyiology[135]. These toxins have an AB structure–function organization, where the A domain encodes the catalytic function of a host macromolecule, while the B domain is responsible for receptor recognition. Toxins employ hydrogen bonding and aromatic stacking to stabilize interactions with sugars[136]. Cross-linking gangliosides or binding a secondary receptor is often necessary to enter host cells. After the endocytosis occurs, the toxin must escape from the endosomes into another intracellular compartment or to the cytosol to exert its effect. As previously mentioned, the pentameric cholera toxin B subunit binds a single class of gangliosides (GM1), while other toxins can bind multiple species with various affinities.[137] Pertussis toxin and ricin show promiscuity binding specific carbohydrate moieties on both glycoproteins and glycolipids[138, 139]. Building on this, a cell delivery method was reported, where nanoparticles were encapsulated within a lipid bilayer and then modified with the cholera toxin B subunit resulting in enhanced motoneuron uptake[140]. Helenius and co-workers showed that murine polyomavirus enter cells via targeting gangliosides. Utilizing a ganglioside-deficient cell line the binding and entry of the used virus-like particles decreased, while addition of gangliosides GM1, GD1a, GT1b to the cells restored cellular uptake[141]. A major preliminary result related to the work presented here was achieved by Matsubara and co-workers[15]. An artificial pentadecapeptide, which binds ganglioside GM3 was identified and shown to internalize avidin and GFP proteins via caveolae/lipid raft-mediated endocytosis.

3. Experimental methods

3.1. Synthesis and purification of peptides

Peptide amides were synthesized manually by SPPS, according to the Fmoc strategy using Tentagel R RAM resin (capacity: 0.19 mmol g^{-1}). The Fmoc protecting groups were removed by using 2% piperidine and 2% 1,8-diazabicycloundec-7-ene (DBU) in *N*,*N*-dimethylformamide (DMF) (5+15 minutes). Washing procedures were carried out with DMF, dichloromethane (DCM), and methanol. Peptide chain elongation was done by activating a three-fold excess of *N*-Fmoc-protected amino acids with 1-[bis(dimethylamino)methylene]-1*H*-1,2,3-triazolo[4,5-*b*]-pyridinium-3-oxide hexafluorophosphate (HATU)/*N*,*N*-diisopropylethylamine (DIEA) in DMF for 3 hours. For the PEG-based construct, Fmoc-Ebes was coupled three times consecutively after the peptide sequence. Efficiency of the coupling steps was monitored with the Kaiser test. The peptides were cleaved from the resin with a mixture of trifluoroacetic acid (TFA)/H_2O/1,4-dithiotreitol (DTT)/triisopropylsilane (TIS) (90:5:2.5:2.5) at room temperature for 3 hours. After TFA was evaporated, peptides were precipitated in ice-cold diethyl ether. The resin was washed with acetic acid and water and subsequently filtered and lyophilized. Peptides were purified on a preparative (250 × 21.2 mm) RP-HPLC column. According to the hydrophobicity and the size of the molecules, Phenomenex Luna (particle size: 10 μm, pore size:100 Å), C18 or Jupiter (particle size: 10 μm, pore size: 300 Å), and C4 or C18 were applied with the appropriate gradient elution using the following eluents: (A) 0.1% TFA in water and (B) 0.1% TFA in acetonitrile/water (80/20). Peptide purity, confirmed by analytical RP-HPLC and ESI-MS measurements, was above 95% for all compounds.

3.2. Isothermal titration calorimetry

ITC was performed in pH 7.2 phosphate buffer solution using a MicroCal VP-ITC microcalorimeter. In individual titrations, 15 μL of solution containing GM1:DPC 1:5 was injected into the ligand solution in the cell (the GM1:DPC mixture was prepared in the same buffer as the ligand in the cell) from a computer-controlled 300 μL microsyringe at intervals of 300 s. All measurements were conducted at 35 °C. The concentration of the ligand in the cell was 15 μM, and the concentration of the ganglioside in the syringe was 300 μM. Control experiments were performed by injecting the ganglioside into a cell containing buffer but no ligand. The experiments were repeated twice. Occasionally tailing heat response curves were observed in both the actual

titrations and background measurements. To test the effects of the tailing on the fitted parameters, specific titrations were repeated with 600 s time delay between injections. Fitted affinity parameters did not exhibit marked change with the experimental setup, indicating that the tailing is not related to the binding phenomenon. After background subtraction and spline baseline correction, the experimental data were fitted to one-binding-site or two-independent-site models (adjustable parameters: ΔH_{b1}, K_{d1}, n_1, and ΔH_{b2}, K_{d2}, n_2) using a generalized reduced gradient nonlinear least-squares procedure. Residual heat of mixing was observed in the enthalpograms due to the inert counter ions and residual solvent in the peptide, protein, and lipid samples, which was corrected by including a constant correction term as an additional fitted parameter. Errors were calculated by jackknife resampling.

3.3. NMR experiments

The ^{1}H and STD NMR spectra were recorded on a Bruker AVANCE III 600 MHz spectrometer equipped with a 5 mm CP-TCI triple-resonance cryoprobe at 308 K. The compounds were dissolved in *d_{18}*-HEPES buffer (20 mM, pH 6.5) containing 10% D_2O. ^{1}H STD spectra were acquired with water suppression using excitation sculpting with pulsed gradients. For the ^{1}H and STD measurements, the ligand concentrations were either 20 or 50 μM with varied GM1 concentrations. The samples were placed in 2.5 mm capillary NMR tubes. As a reference, STD experiments were also performed without the target in samples that contained the ligand species alone. STD NMR spectra were acquired using a series of 40 equally spaced 50 ms Gaussian-shaped pulses for selective saturation of the protein, with a total saturation time of 2 s and a 50 ms spinlock to suppress the signal from the bicelles. The frequency of the on-resonance saturation was set at 1.2 ppm, and the off-resonance saturation frequency was set at 40.0 ppm. A total of 8k scans were collected for each pseudo-2D experiment.

3.4. Tryptophan fluorescence blue-shift measurements

Fluorescence experiments were carried out using a Hitachi F-2500 fluorescence spectrophotometer (PMT voltage: 700 V, response: 0.08 s) at room temperature, in 20 mM PBS (pH 7.4). Tryptophan excitation was performed at 295 nm. Emission spectra were recorded from 300 to 400 nm and the excitation and emission bandwidths were set at 5 nm. Peptides were measured alone (2.5 μM) and with the addition of either 250 μM DPC micelles or 50 μM GM1:250

μM DPC bicelles. Control measurements without the peptide were subtracted from the corresponding measurement data.

3.5. Circular dichroism

Circular dichroism measurements were performed by using a Jasco J-815 CD Spectrometer. CD spectra were recorded by using a thermally jacketed 1 mm quartz cuvette, from 260 to 195 nm, at a scan speed of 50 nm min^{-1}, with 5 accumulations. Compounds were dissolved in 10 mM PBS (pH 7.4) with peptide concentrations of 200 μM. The effect of the ganglioside was measured with the addition of 100:500 μM of GM1:DPC bicelles. For thermal control, a Julabo water thermostat was used with a 10-min equilibration time at each temperature. The solvent baseline was subtracted.

3.6. Cell cultures

HeLa cells were cultured in advanced MEM (Gibco, Life Technologies) supplemented with 10% fetal bovine serum (FBS, PAN Biotech). JN_2B_4D Jurkat cells were cultured in RPMI-1640 medium (Gibco) supplemented with 5% FBS. Both media contained penicillin-streptomycin (100 U mL^{-1}, Gibco) and 2 mM L-glutamine (Gibco). The cells were grown in a humidified incubator containing 5% CO_2 at 37 °C.

3.7. Preparation of the carrier–protein complexes

To prepare peptide–NeutrAvidin complexes, biotinylated peptides were incubated with FITC–NeutrAvidin in cell culture medium at a molar ratio of 4:1. The resulting solution containing the complexes was added to the cells at various concentrations. To prepare the antibody complexes, a solution of the biotinylated peptide was mixed with biotinylated monoclonal mouse anti-human galectin-1 (2c1/6) antibody[142] and labeled or unlabeled NeutrAvidin at a molar ratio of 3:1:1; secondary r-phycoerythrin-conjugated goat anti-mouse IgG (F-(ab')2, DakoCytomation) or in some cases secondary AlexaFluor 647-conjugated F(ab′)2-goat anti-mouse IgG (Invitrogen) antibody was then added to the solution at a 1:1 molar ratio with the primary antibody. HeLa cells were incubated with various concentrations of this complex.

3.8. Flow cytometry

The internalization of peptides and peptide–NeutrAvidin complexes was determined by flow cytometric analysis. Cells (6×10^4 in 24-well plates) were grown at 37 °C for 24 h. After

removal of the medium, the cells were washed with PBS and incubated with peptides or peptide complexes in MEM + 1% FBS at 37 °C. The cells were then washed with PBS, harvested from the plates with 0.05% trypsin-EDTA, and washed with PBS. Trypan blue (Reanal) and propidium iodide (Fluka) were added to the cells at final concentrations of 0.1% and 15 μM, respectively, in PBS immediately before the cells were subjected to flow cytometric analysis (FACSCalibur flow cytometer, BD Biosciences). The data were evaluated using FlowJo™ software (FlowJo, LLC). The fluorescence intensity of control cells and that of the FITC–NeutrAvidin, respectively, were subtracted from the fluorescence intensity of the peptides and peptide–NeutrAvidin complexes. For the measurement of ganglioside GM1 content, HeLa and Jurkat cells were incubated with 8 μM FITC-cholera toxin B subunit on ice for 30 min and then subjected to flow cytometric analysis as described above. For the *in vitro* competition assay, Jurkat cells were treated with 1 μM peptide alone or with 1, 5 or 10 μM galectin-1. For the endocytosis inhibition experiments, HeLa cells were preincubated at 37 °C with 5 mg mL^{-1} methyl-β-cyclodextrin (MBCD) for 60 min, 10 μM wortmannin for 60 min, or 10 μg mL^{-1} chlorpromazine for 30 min. The cells were then incubated with 1 μM peptide–NeutrAvidin complexes at 37 °C for 60 min, treated with trypan blue, and subjected to flow cytometric analysis as described above. All experiments were performed in triplicate.

3.9. Live confocal laser scanning microscopy

HeLa cells were plated overnight culturing in MEM+10% FBS at 1.25×10^4 cells per cm^2 (or 1.5×10^4 cells per channel) on 6-chamber μ-Slides VI 0.4 (ibidi). The cells were washed with PBS and incubated with the studied complexes in MEM+1% FBS medium at different concentrations for different incubation times at 37 °C. The cells then were washed with PBS. When antibody-complexes were used, they were also washed with 100 mM β-lactose (Sigma-Aldrich) and the biotinylated peptide–NeutrAvidin complex without the primary and secondary antibody to remove surface-bound complexes. The cells were stained with 100 ng mL^{-1} Hoechst 33342 (Sigma-Aldrich) in MEM medium for 30 min at 37 °C. In some experiments, after Hoechst staining, the cells were labeled with LysoTracker Red (Life Technologies) at 75 nM for 30 min at 37 °C according to the manufacturer's instructions. For the cholera toxin colocalization experiments, cells were co-incubated with 5 μM FITC labeled CTX-B subunit (Sigma-Aldrich). For the structural test of the antibody complex, cells were treated with the complex for 3 h at 500

nM then the cells were fixed with 1.6% paraformaldehyde for 15 min at room temperature, permeabilized with 0.01% saponin for 10 min, and then cells were stained with 350 nm Atto 488-conjugated galectin-1 for 30 min at room temperature. For the IgG complex measurements, cell membranes were visualized after a 5-minute treatment with FITC-labeled WGA lectin at 0.2 μg ml^{-1} at room temperature after incubation with the complex. The cells were incubated in Leibovitz's L-15 medium (Life Technologies) during microscopic analysis. FITC–NeutrAvidin complexes were treated with 0.1% Trypan blue to quench extracellular fluorescence. To observe the localization of the cargo, cell fluorescence was analyzed using a Leica SP5 AOBS confocal laser scanning microscope using the 405 nm UV diode (for Hoechst staining), the 488 nm argon laser line (for FITC and Atto 488 staining), the 543 nm HeNe laser line (for r-phycoerythrin and LysoTracker Red staining), and the 633 HeNe laser line (for Alexa Fluor 647 staining). For emission detection, an appropriate spectral filter was used for each channel.

3.10. Image analysis

To identify cells and extract their properties, we used maskRCNN[143], a deep learning-based image segmentation platform, U-Net[144], another deep learning approach, and CellProfiler[145] software for feature extraction. First, cell nuclei were identified based on the Hoechst signal using a very heavily augmented training set of The Data Science Bowl 2018 competition. The augmentation was performed by learning image styles and generating synthetic images of similar types with Pix2pix, a GAN (generative adversarial network) deep network[146]. A maskRCNN network was then trained, and individual nuclei were inferred. A similarly augmented image set of our experiment was used to train a U-Net deep convolutional neural network, using the FITC-WGA lectin channel images and binary masks marking the cytoplasms as foreground. The trained U-Net network predicted the foreground pixels corresponding to cytoplasms. The cytoplasm was approximated with a Watershed region propagation algorithm on the weighted sum image of the U-Net prediction and the FITC-WGA lectin channel. Using the detected objects (nucleus and cytoplasm) as masks, cellular features such as r-phycoerythrin intensity values, textural properties, and morphological descriptors were extracted. For the final statistical analysis, the integrated intensities of individual cells were used.

3.11. Cytotoxicity assay

The kinetics of cell reaction to peptide treatment were monitored by impedance measurement at 10 kHz (RTCA-SP instrument, ACEA Biosciences, San Diego, CA, USA). Impedance measurement is noninvasive, label-free, and real-time and correlates linearly with the adherence, growth, number, and viability of the cells. For background measurements, 50 μL of cell culture medium was added to the wells, and HeLa cells were seeded at a density of 6×10^3 cells/well on noncoated 96-well plates with integrated gold electrodes (E-plate 96, ACEA Biosciences). At the beginning of the plateau phase of growth, the cells were treated with peptide solutions at 0.1, 0.5, 1, 5, and 10 μM, and the effects of treatment were followed for 24 hours. Triton X-100 detergent (1 mg mL^{-1}) was used as a reference compound to induce cell death. The cell index was defined as Rn-Rb at each time point of measurement, where Rn is the cell-electrode impedance of the well when it contains cells and Rb is the background impedance of the well containing medium alone.

3.12. Statistical analysis

Statistical analysis included one-way analysis of variance (ANOVA) with post hoc Tukey honestly significant difference test (*, $p < 0.1$; **, $p < 0.01$; ***, $p < 0.001$; ****, $p < 0.0001$) and unpaired Student's t-test (*, $p < 0.05$; **, $p < 0.01$; ***, $p < 0.001$; ****, $p < 0.0001$).

4. Results and discussion

4.1. Biophysical characterization of the WYKYW–GM1 binding

A pentapeptide family containing Tyr-Xxx-Tyr was identified by Gabius and coworkers as carbohydrate mimetics binding various lectins.[147–149] A member of this family, our lead molecule, WYKYW (Trp-Tyr-Lys-Tyr-Trp-NH_2) was observed to decouple galectin-1–proteoglycan interactions. The experimental setup suggested this peptide being a lectin ligand. With the use of saturation transfer difference (STD) and transferred nuclear Overhauser effect (trNOE) nuclear magnetic resonance (NMR) measurements, our research group showed that this decoupling arises from the competitive binding of the pentapeptide and the galectin-1 at the glycan moiety of asialofetuin.[150] Starting from this experiment, and knowing that ganglioside GM1 is the major receptor of galectin-1, we hypothesized an interaction between WYKYW and the carbohydrate moiety of GM1 (Figure 7).[151]

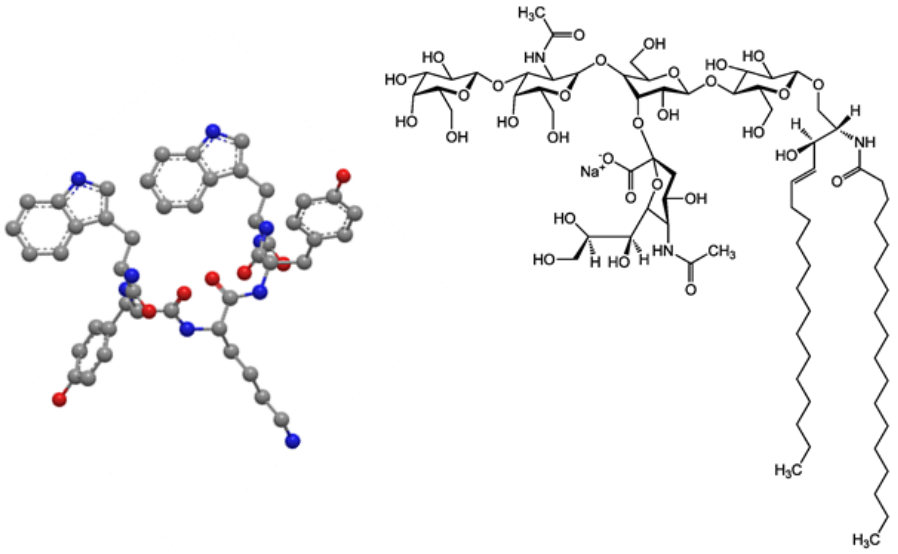

Figure 7. Lead molecule WYKYW (left) and its target ganglioside GM1 (right).

To that end, the pentapeptide and its derivatives were synthesized with Fmoc chemistry, purified with HPLC, and their affinity and specificity to different gangliosides were measured using isothermal titration calorimetry (ITC) and NMR. The role of membrane components in the binding phenomenon was also studied using ITC, NMR, and tryptophan fluorescence measurements.

4.1.1. High affinity and specificity

The affinity and specificity of the pentapeptide to three different gangliosides were measured. These are ganglioside GM1, ganglioside GM3, which lacks the terminal β-D-Gal(1→3)GalNAc moiety, and asialo-GM1, which lacks the sialic acid (Figure 8).

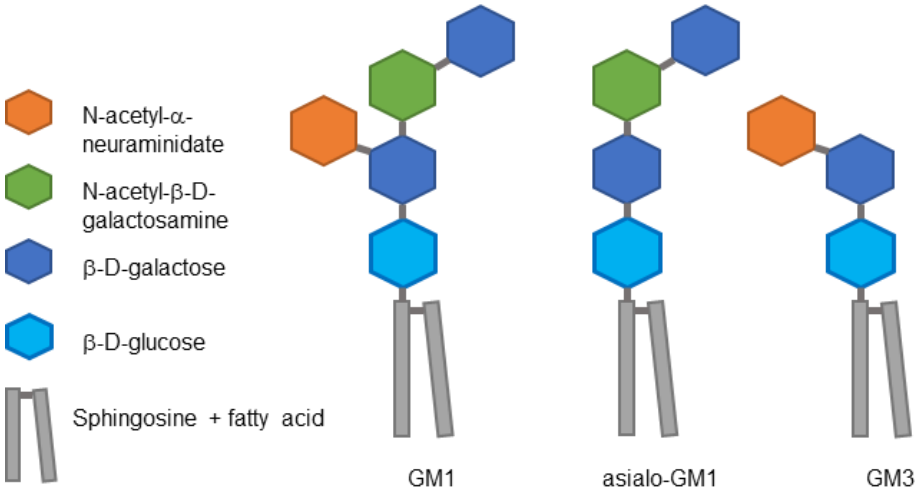

Figure 8. Structures of the examined ganglioside derivatives.

Effective signal attenuation and broadening was observed upon mixing WYKYW with GM1:*n*-dodecylphosphocholine (DPC) bicelles[152], indicating a strong interaction (Figure 9).

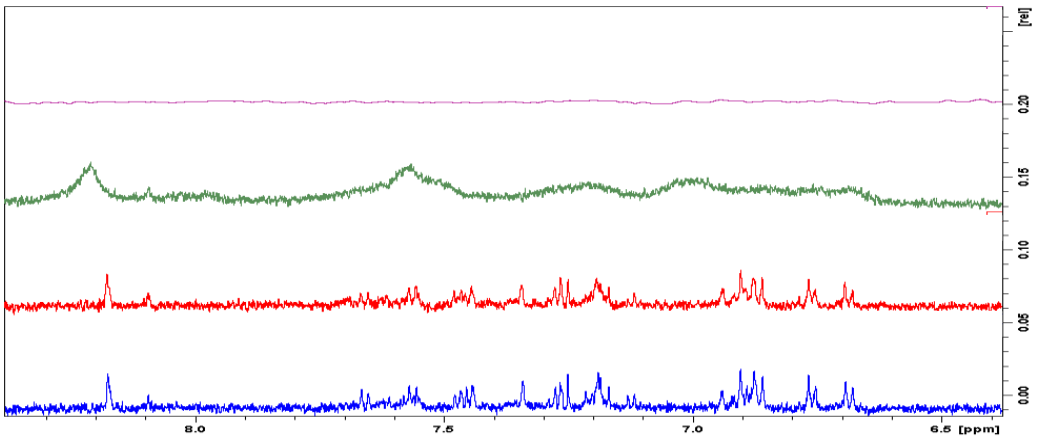

Figure 9. NMR detection of the WKYKW–GM1 interaction: ^{1}H STD of 20 μM WYKYW + 100 μM DPC + 20 μM ganglioside GM1 (purple), ^{1}H NMR of 20 μM WYKYW + 100 μM DPC + 20 μM ganglioside GM1 (green), ^{1}H NMR of 20 μM WYKYW + 100 μM DPC (red), ^{1}H NMR of 20 μM WYKYW (blue).

Ganglioside GM3 showed partial line broadening in the ^{1}H NMR spectrum, and STD signals could be observed, which indicated an elevated exchange rate, pointing to a weak binding

phenomenon. Removing the sialic acid was detrimental to the binding and left NMR spectra intact, without any observable saturation transfer difference (Figure 10). In the control measurement, when gangliosides were excluded and only pure DPC was used, no interaction was found.

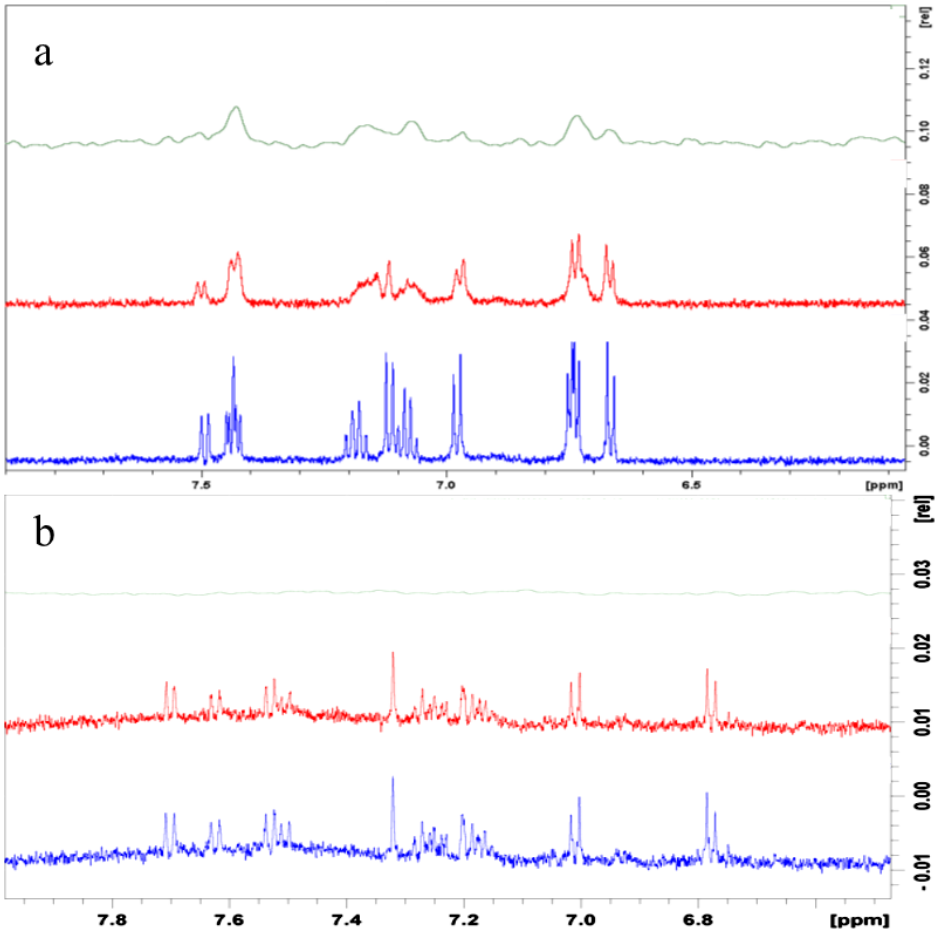

Figure 10. NMR detection of the (**a**) WKYKW–GM3 and (**b**) WKYKW–asialo-GM1 interaction: ^{1}H STD of 20 µM WYKYW + 100 µM DPC + 20 µM ganglioside (green), ^{1}H NMR of 20 µM WYKYW + 100 µM DPC + 20 µM ganglioside (red), ^{1}H NMR of 20 µM WYKYW (blue).

The interactions were confirmed by isothermal titration calorimetry. In the case of WYKYW, a two-stage interaction was found (Figure 11). The first binding step displayed a low nanomolar affinity with a GM1:WYKYW stoichiometry of 1:2, while the second stage was a micromolar interaction. Supporting the NMR measurements, the interaction with ganglioside GM3 was weak, while asialo-GM1 and the control DPC micelles showed no binding.

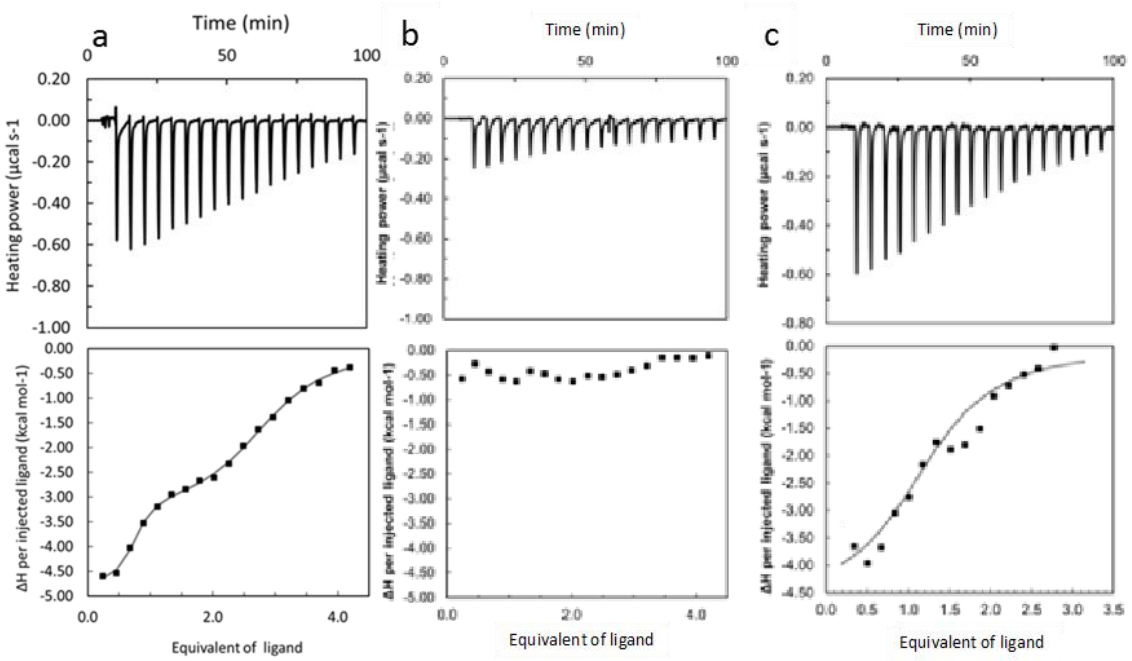

K_{D1} (nM)	23.8 ± 5.5	not fittable	3063 ± 150
K_{D2} (nM)	1647 ± 109		n.a.
n_1	0.55 ± 0.02		1.16 ± 0.01
n_2	1.92 ± 0.02		n.a.

Figure 11. ITC enthalpograms for WYKYW with (**a**) GM1, (**b**) asialo-GM1, and (**c**) GM3. Titrations were conducted with ganglioside:DPC 1:5 bicelles (solid square), and nonlinear least-squares fitting was performed against the two-independent-binding-site model (solid lines). Binding affinites (K_D) and stoichiometries (n) are indicated in the corresponding table column.

4.1.2. Structural requirements of the binding

We utilized a medicinal chemistry approach to set up a structure–affinity relationship. To determine the required side chains, we performed an alanine-scan, substituting each of the five amino acids one by one, and measured ITC with GM1:DPC bicelles. This revealed that any side chain missing from the original sequence can be detrimental to binding. To get a picture about the optimal configuration of the amino acids, D-amino acid substitution was carried out. We hypothesized that the high-affinity WYKYW–GM1 interaction needs precise fitting of the two molecules, and the scan confirmed this notion. That is no change in the amino acid configuration is tolerable, which strengthens the concept of molecular recognition between the sequence and the ganglioside. Backbone homologation with β-amino acids, however, yielded sequences with

comparable or even better affinities, which tells us that there is room for improvement by backbone homologation, which can also improve enzymatic stability (Table 1).

Table 1. Binding affinities (K_D) of the first binding-step in nM of the original pentapeptide substituted in various manners. The binding stoichiometry (n_1) was 0.5 in all cases.

	^{N}**W**	**Y**	**K**	**Y**	**W**^{C}
original			23.8		
Ala-scan	not fittable	5755	10467	1694	1060
β-scan	4.3	60	332	40	86
D-scan	881	892	4523	3243	3926

To test the internalization of the peptide, peptides tagged with 5(6)-carboxyfluorescein (CFU) were synthesized. Proximity of the fluorescein moiety to the pentapeptide decreased binding; therefore, it was not the preferred setup (Figure 12).

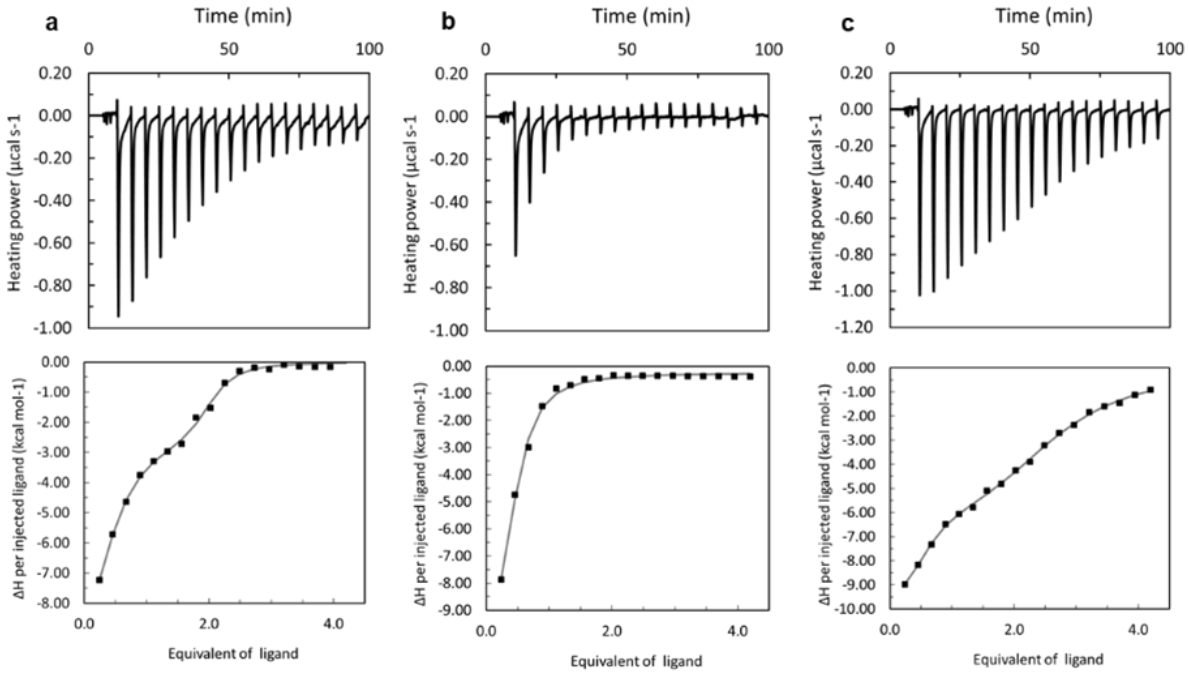

Figure 12. ITC detection of interactions of GM1 with CFU-tagged WYKYW derivatives. Enthalpograms of (**a**) peptide CFU-WYKYW (n_1 = 0.5, K_{D1} = 163.94 nM, n_2 = 1.5, K_{D2} = 1379.26 nM), (**b**) peptide CFU-WYKYW-GG-Penetratin (n=0.5, K_D= 894 nM) and (**c**) peptide CFU-Penetratin-GG-WYKYW (n_1 = 0.5, K_{D1} = 152 nM, n_2 = 1.78 K_{D2} = 3420 nM). Titrations were carried out with GM1:DPC 1:5 bicelles.

To overcome this, we selected NeutrAvidin (NA) labeled with fluorescein isothiocyanate (FITC) as a model cargo and tagged it with a biotinyl-PEG-WYKYW conjugate, where PEG designates a trimeric linker obtained by coupling 8-amino-(3,6-dioxa-octyl)succinamic acid monomers. As NeutrAvidin binds four biotinylated sequences, a tetravalent protein construct was obtained [NA(biotinyl-PEG-WYKYW)$_4$] (Figure 13). To compare the performance and efficiency of WYKYW relative to a reference cell-penetrating archetype, FITC-NA was tagged with biotinyl-Penetratin (RQIKIWFQNRRMKWKK), yielding NA(biotinyl-Penetratin)$_4$. The additive and synergistic effects of WYKYW and Penetratin were to be measured with chimaera construct NA(biotinyl-Penetratin-GG-WYKYW)$_4$.

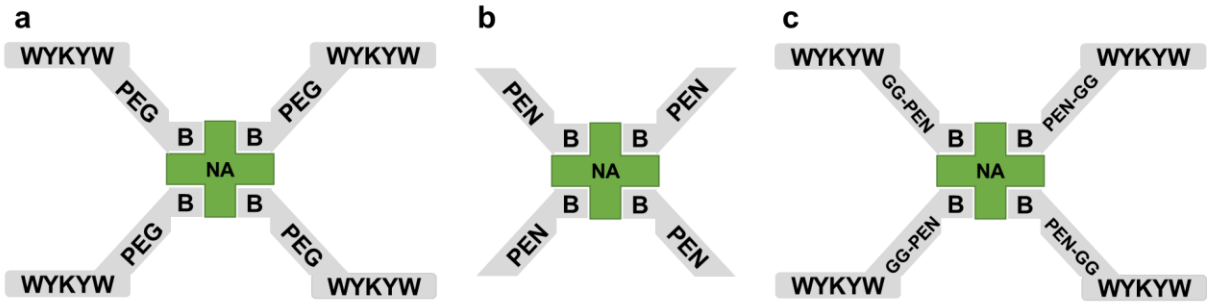

Figure 13. Schematic representation of (**a**) NA(biotinyl-PEG-WYKYW)$_4$, (**b**) NA(biotinyl-Penetratin)$_4$ and (**c**) NA(biotinyl-Penetratin-GG-WYKYW)$_4$.

ITC measurements confirmed that NA(biotinyl-PEG-WYKYW)$_4$ and NA(biotinyl-Penetratin-GG-WYKYW)$_4$ bound GM1 with K_Ds of 14.5 ± 1.7 and 20.8 ± 2.7 nM, respectively (Figure 14). The stoichiometry of the interaction was 1:1 under conditions of excess of the tagged protein. NA(biotinyl-Penetratin)$_4$ displayed no affinity towards GM1.

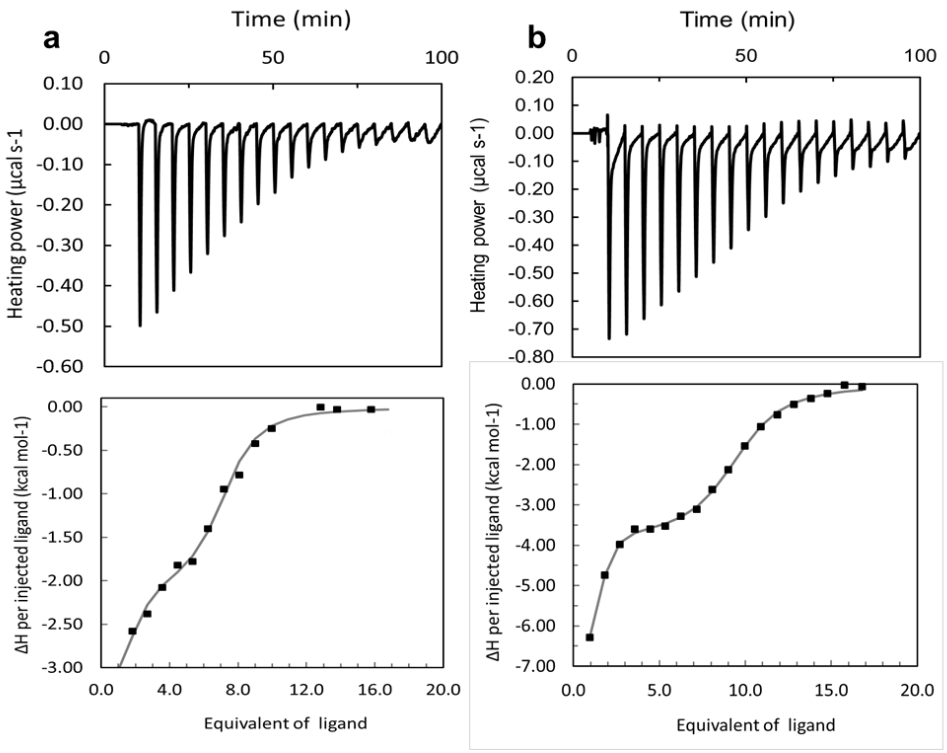

Figure 14. ITC enthalpograms for (**a**) NA(biotinyl-PEG-WYKYW)$_4$ and (**b**) NA(biotinyl-Penetratin-GG-WYKYW)$_4$. Titrations were conducted with GM1:DPC 1:5 bicelles (solid square), and nonlinear least-squares fitting was performed against the two-independent-binding-site model (solid lines).

4.1.3. The role of membrane components

The presence of the Trp residues at the termini led us to hypothesize the important role of the membrane in the interaction[153]. As previously shown, interaction with pure DPC membrane indicated no binding phenomenon. However, NMR and ITC experiments carried out with the GM1 pentasaccharide moiety without the hydrophobic part responsible for membrane insertion showed no binding (Figure 15). This strongly suggested that both sphingosine and fatty acid moieties contribute to the binding surface. Circular dichroism showed intensity loss at 198 nm upon the addition of the GM1:DPC bicelles. Evaluating the CD spectra is not obvious, because of the excess of aromatic rings present interference with the peptide bands in the far-UV region; however, the intensity change can indicate interactions between tyrosine residues and the ganglioside (Figure 16). Along with the NMR results, it is most likely that tryptophan face-to-edge interactions occur in solution, which are then disassembled as the binding occurs. To test the interaction between aromatic rings, two disubstituted peptides, WAKAW and AYKYA were synthesized. The

intensive peak at 198 nm could be identified as a tryptophan band, which showed a minimal blue-shift and a significant intensity loss upon interacting with tyrosines. Interestingly, both WAKAW and AYKYA peptides have a strong positive peak at 227 nm, which showed elevated intensity and red-shifted to 230 nm, when both types of aromatic side chains were present. Tryptophan fluorescence blue-shift was measured in the presence of DPC micelles and GM1:DPC bicelles.

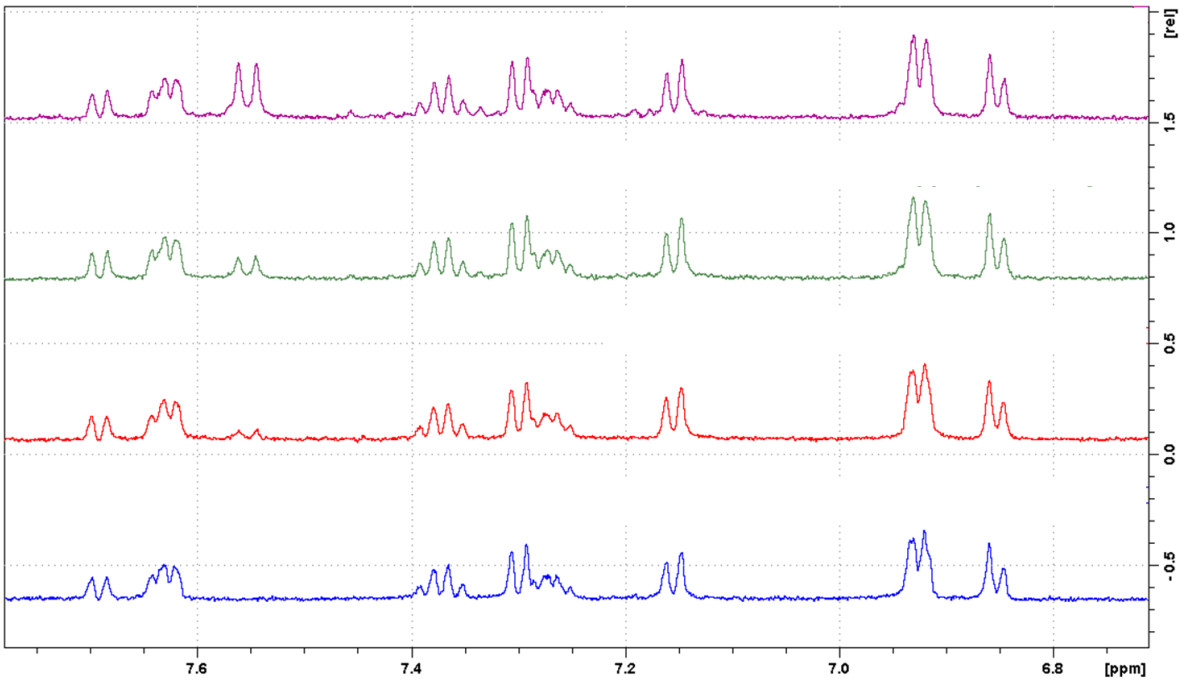

Figure 15. NMR detection of the WKYKW–GM1 pentasaccharide interaction: ^{1}H NMR of 50 μM WYKYW (blue), ^{1}H NMR spectra of 50 μM WYKYW + 25 μM (red) / 50 μM (green) / 100 μM (purple) pentasaccharide.

WYKYW and all β-substituted analogues alone had an emission maximum at 350 nm. Addition of DPC micelles did not change the maximum and only slightly changed the intensity. In contrast, the addition of GM1:DPC bicelles blue-shifted the emission maximum to 341 nm together with a huge increase of intensity. The shift of the fluorescence peak indicates that tryptophan became more buried and shielded. The magnitude of the shift is consistent with a relative permittivity of 7, which means that tryptophans neither reside in the solvent, nor buried in the hydrophobic interior, but they are located near the headgroups of the amphipathic molecules.[154] Our hypothesis is that the WYKYW peptide has no ordered structure in the aqueous phase, but binding its target ganglioside can induce the formation of a beta-sheet-like motif, which enables a

single peptide sequence to recruit multiple gangliosides, resulting in the activation of endocytic mechanisms.

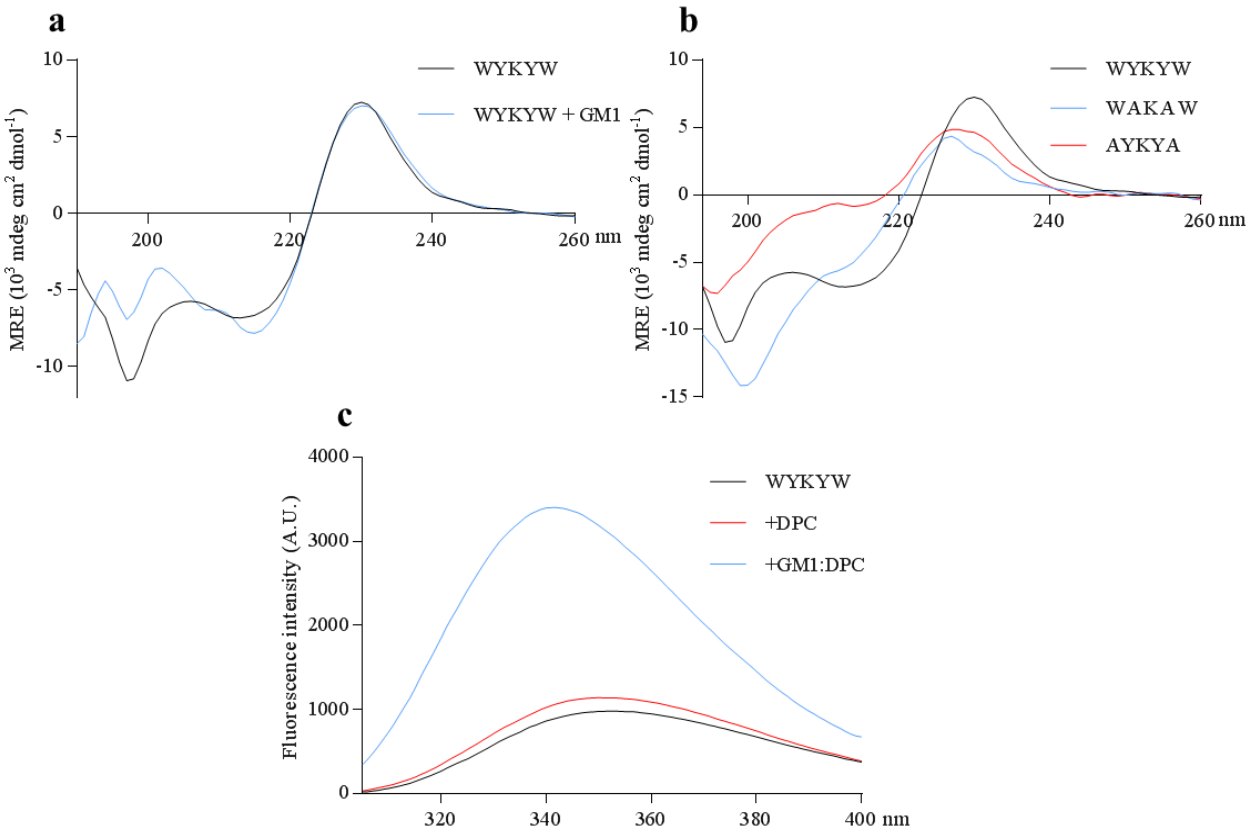

Figure 16. (**a**) CD spectrum of the peptide WYKYW alone (black, 200 μM) and with 100:500 μM GM1:DPC (blue) bicelles at 303 K. (**b**) CD spectrum of peptides WYKYW, WAKAW, and AYKYA (200 μM) at 303 K. (**c**) Tryptophan emission blue-shift measurement comparing the peptide WYKYW alone (black, 2.5 μM), with WYKYW+DPC (DPC 250 μM, red), and WYKYW+GM1:DPC (GM1:DPC 50:250 μM, blue).

4.2. Endocytosis-inducing properties of the WYKYW tag

4.2.1. Lipid raft-mediated endocytosis

To test the entry of any cell delivery system into the cells, one must exclude techniques, which utilize fixation and permeabilization methods, because these can yield false positive results.[155] Unfortunately, the discovery of these artefacts questioned all cell-penetrating peptide mechanisms examined previously, and research groups had to reevaluate their experimental observations.[156] To overcome this issue, live confocal laser scanning microscopy (CLSM) experiments were conducted with the previously described constructs (Figure 13). Both

NA(biotinyl-PEG-WYKYW)$_4$ and NA(biotinyl-Penetratin-GG-WYKYW)$_4$ showed effective uptake at an extracellular cargo concentration in the range of 250 nM to 1000 nM. Much to our surprise, NA(biotinyl-Penetratin)$_4$ could not enter the cells under these conditions (Figure 17).

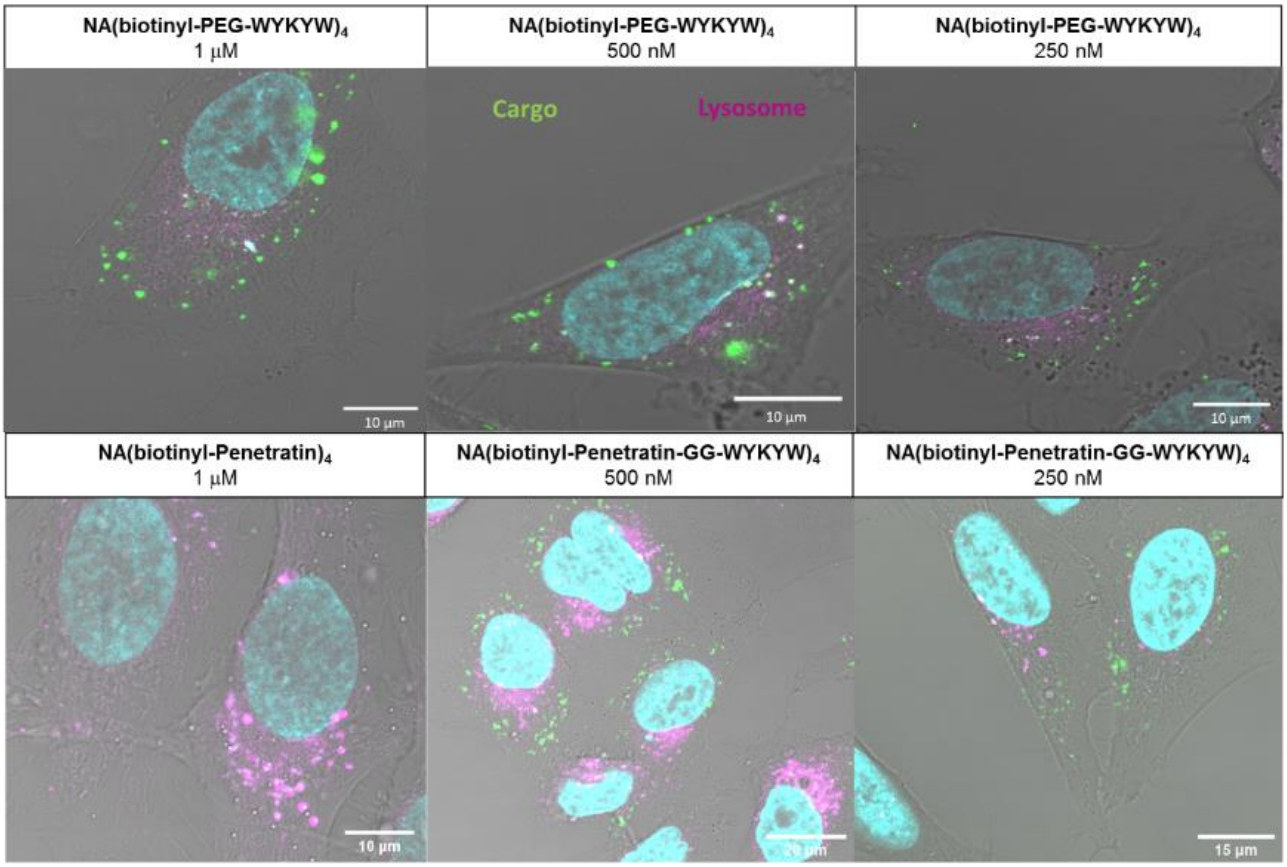

Figure 17. Internalization of the constructs at different concentrations by HeLa cells after 6 hours as determined by live confocal laser scanning microscopy. FITC-labeled NeutrAvidin is shown in green, Hoechst 33342-stained nuclei are shown in cyan, and LysoTracker Red-stained lysosomes are shown in magenta.

To quantify the internalization of the carrier–cargo constructs, fluorescence-activated cell sorting (FACS) measurements were conducted. The extracellular cargo concentration was kept at 1 μM, and trypan blue was used to quench the fluorescence of membrane-bound, but not internalized molecules. Both NA(biotinyl-PEG-WYKYW)$_4$ and NA(biotinyl-Penetratin-GG-WYKYW)$_4$ showed significant uptake, while the control NA(biotinyl-Penetratin)$_4$ was not internalized into the cells, confirming and further validating the CLSM experiments (Figure 18a).

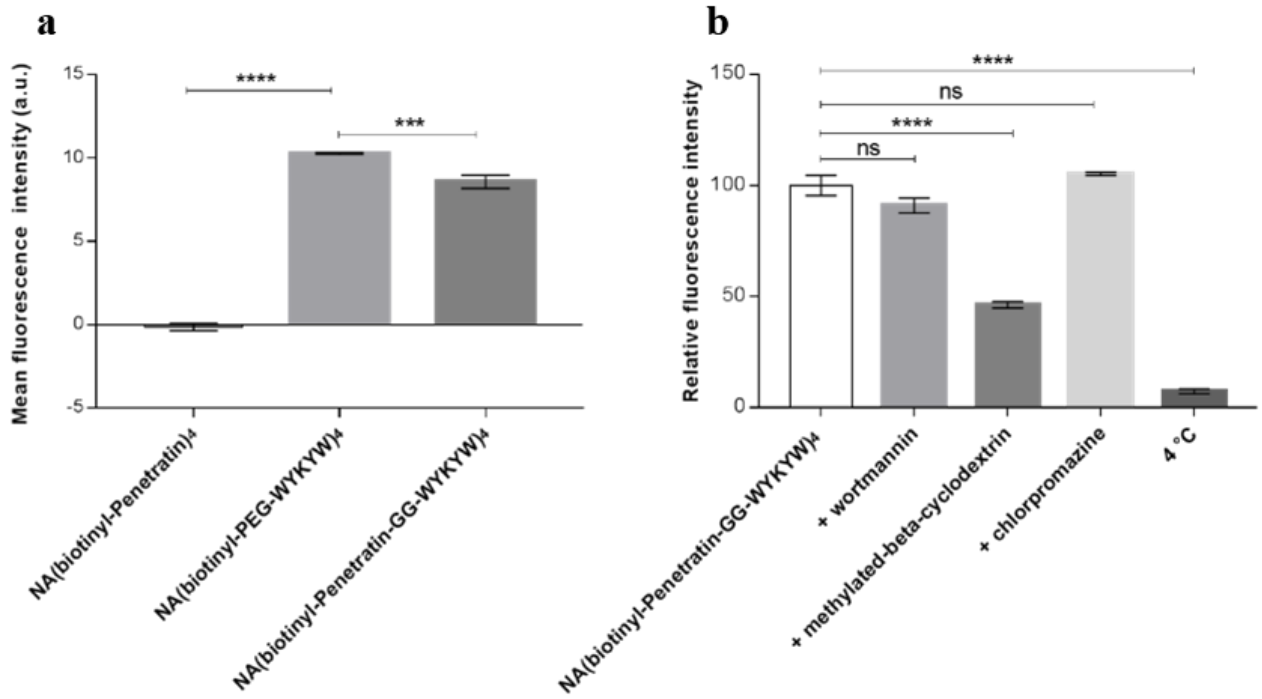

Figure 18. (**a**) Internalization of the constructs at 1 μM by HeLa cells after 1 hour as determined by flow cytometry. (**b**) Influence of endocytosis inhibitors on cellular uptake as determined by flow cytometry. HeLa cells were preincubated with the inhibitors wortmannin, chlorpromazine, or methyl-β-cyclodextrin at 37 °C for 30 or 60 min and subsequently incubated with NA(biotinyl-Penetratin-GG-WYKYW)$_4$ at 37 °C for 60 min. A control experiment was also performed at 4 °C. Each data point depicts the mean of three measurements; the error bars show the standard error of the mean. Statistical analysis was performed using one-way analysis of variance (ANOVA) with post hoc Tukey HSD. *, $p < 0.1$; **, $p < 0.01$; ***, $p < 0.001$; ****, $p < 0.0001$.

These experiments suggested that the GM1 recognition sequence WYKYW was able to trigger internalization when attached to a model protein (63 kDa) through a linker. In contrast, penetratin did not induce the uptake of the cargo under these conditions. It is worth to note, that penetratin in the literature is usually used at higher (10–40 μM) concentrations.[157] No additive or synergistic effects were found. In fact, the presence of penetratin in the carrier sequence reduced the uptake efficiency compared to that of the PEG linker derivative, indicating that WYKYW alone has a reliable uptake-inducing effect that is independent of the linker chemistry applied.

To validate the supposed endocytic mechanism, we performed endocytosis inhibition experiments with NA(biotinyl-Penetratin-WYKYW)$_4$. The internalization of the complex could be blocked at low temperature (4 °C), which proves the energy dependency of the translocation,

which is a well-known feature of endocytosis. Preincubating the cells with various endocytosis inhibitor molecules, a significantly decreased entry of the complex was observed in the case of methyl-β-cyclodextrin, a well-known lipid raft inhibitor. The macropinocytosis and clathrin-mediated endocytosis inhibitors chlorpromazine and wortmannin had no significant effects (Figure 18b). To gain additional supporting evidence of the lipid raft-mediated pathway, a co-localization experiment was carried out. A carrier–cargo complex tagged with Alexa Fluor 647 secondary antibody was utilized, and its co-localization with FITC-labeled cholera toxin B subunit was observed in CLSM. Cholera toxin has been reported to enter cells through GM1 binding via lipid rafts. Strong correlation was found between the signals of cholera toxin and our carrier–cargo complex, indicating that WYKYW induces lipid raft-mediated endocytosis, consistent with the fact that GM1 is localized in lipid rafts and caveolae (Figure 19).

Figure 19. Co-localization after internalization of the carrier [NA(biotinyl-Penetratin-GG-WYKYW)$_3$]–cargo (biotinylated primary and fluorescent secondary IgGs) complex at 80 nM (indicated in magenta, secondary antibody tagged with Alexa Fluor 647) with the FITC-labeled cholera toxin B subunit at 5 µM (indicated in green) after 1 hour. Nuclei are stained with Hoechst33342 (indicated in cyan).

As mentioned, most cell delivery system fail to deliver cargoes, even if they can successfully achieve endocytosis, because the constructs remain entrapped in endosomes and then they are fused with lysosomes, resulting in degradation of the potentially bioactive cargo. Staining of lysosomes showed no co-localization with our carrier–cargo complex, even after 6 hours, indicating the ability of WYKYW to elude the lysosomal lytic route, which is an attractive feature of certain lipid raft-mediated endocytic pathways (Figure 17).

4.2.2. A single WYKYW copy is enough to induce endocytosis

Earlier studies pointed out that the multivalent binding (clustering) or ganglioside GM1 is necessary to trigger lipid raft-mediated endocytosis. The tetravalent nature of our model delivery system is consistent with this observation. However, if the carrier–cargo complex is produced with recombinant synthesis, and one wants to produce an easy-to-adapt and easy-to-use delivery system, the number of carrier sequence copies required to induce endocytosis is crucial. To that end, a monovalent CFU-Penetratin-GG-WYKYW sequence was synthesized and its uptake was tested. The peptide sequence showed a K_D of 141 ± 45 nM toward ganglioside GM1. Control measurements were conducted using CFU-Penetratin, which showed no binding toward the ganglioside. Cellular uptake by human HeLa and Jurkat cell lines were measured by FACS, with trypan blue as an extracellular fluorescence quencher (Figure 20a).

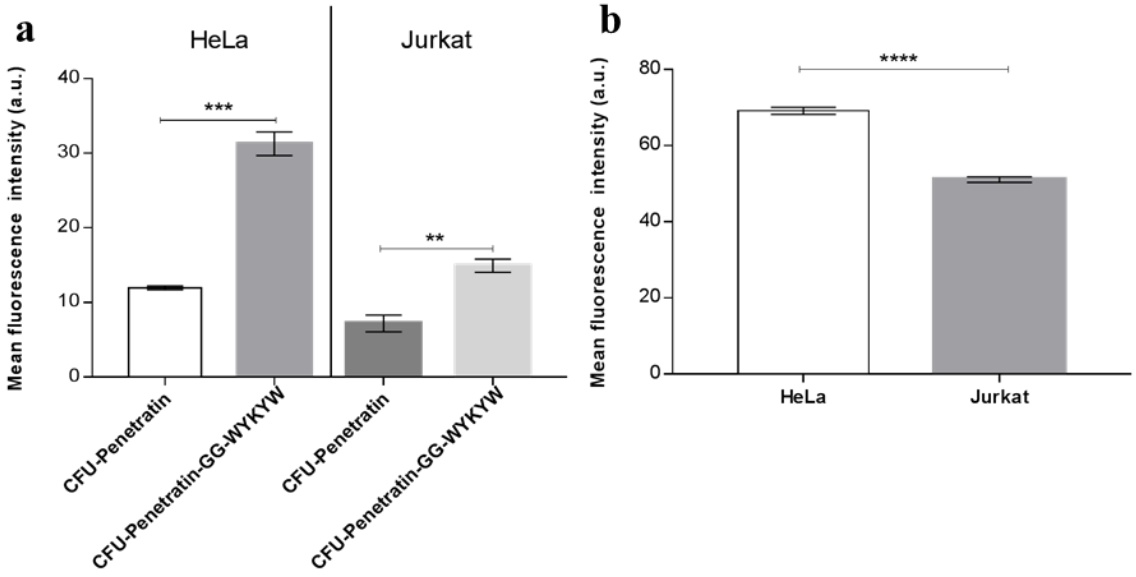

Figure 20. (**a**) Uptake of fluorescently labeled sequences at 1 μM by HeLa and Jurkat cells after 1 hour. (**b**) Cell surface expression of GM1 in HeLa and Jurkat cells measured by FITC-cholera toxin staining. Each data point represents the mean of three measurements, and the error bars show the standard error of the mean. The unpaired Student's t-test was used in the statistical analysis of the data shown: *, $p < 0.05$; **, $p < 0.01$; ***, $p < 0.001$; ****, $p < 0.0001$.

The peptides were applied at an extracellular concentration of 1 μM, which is still an order of magnitude lower than the optimum concentration utilized for penetratin.[158] Nevertheless, without the protein cargo, CFU-Penetratin alone could internalize in our hands. CFU-Penetratin-GG-WYKYW displayed three- and two-fold increases in cell penetration efficiency in the HeLa

and Jurkat cell lines, respectively, compared that that obtained for CFU-Penetratin without the macromolecular cargo. The amount of intracellular cargo was twice as high in HeLa cells as in Jurkat cells. Our hypothesis was that the difference between the two cell lines is related to the cell surface expression level of ganglioside GM1. To test this, binding experiments were performed with cholera toxin B subunit at 4 °C. At this temperature, endocytosis is blocked, and the total GM1 content of the cells can be quantified. This experiment revealed that HeLa cells expressed a higher level of GM1 than Jurkat cells (Figure 20b).

The direct GM1-dependence of endocytosis was further tested with a competition experiment. Galectin-1 binds terminal digalactosides with a micromolar affinity[159] and thus it was used as an inhibitor / competitor molecule of our carrier peptides (Figure 21a). Increasing the concentration of galectin-1 decreased the uptake of CFU-Penetratin-GG-WYKYW, reaching complete inhibition at 10 μM, where only the base level of the internalization of CFU-Penetratin was achieved. It is worth to note, that even though galectin-1 acted as a competitive inhibitor of the WYKYW–GM1 interaction, this occurred only at concentration orders of magnitude higher than the endogenous *in vivo* serum galectin-1 level of 100 ng mL^{-1} (6.7 nM)[160]. Based on this observation, the risk of potential in vivo inhibition of the endocytosis routing effect is low. These findings suggest that a single WYKYW moiety is sufficient to trigger endocytosis through GM1 binding, leading to efficient delivery. The possible cytotoxicity of CFU-Penetratin-GG-WYKYW, biotinyl-Penetratin-GG-WYKYW, and NA(biotinyl-Penetratin-GG-WYKYW)$_4$ was tested at higher concentrations, and it showed no toxicity for HeLa cells at concentrations of up to 10 μM, rendering them safe candidates for further experiments. (Figure 21b).

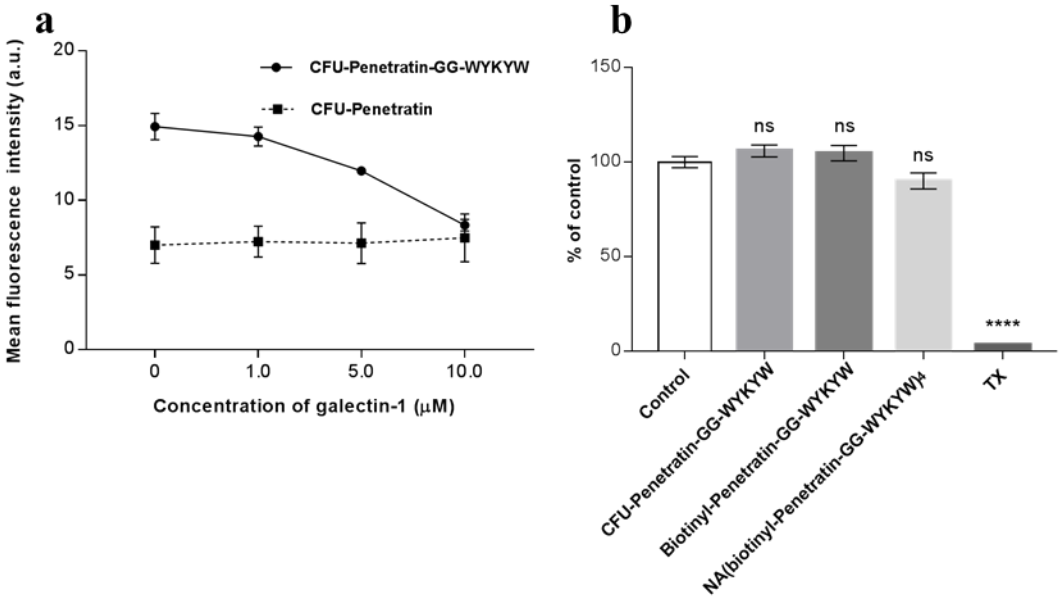

Figure 21. (**a**) Uptake of CFU-Penetratin and CFU-Penetratin-GG-WYKYW at 1 μM in competition with galectin-1 at 0–10 μM. (**b**) Cytotoxicity of CFU-Penetratin-GG-WYKYW, Biotinyl-Penetratin-GG-WYKYW and NA(biotinyl-Penetratin-GG-WYKYW)$_4$ at 10 μM to HeLa cells after 24 hours as determined by bioimpedance measurements. Triton X-100 was used as a toxicity control. Each data point represents the mean of three measurements, and the error bars show the standard error of the mean. One-way analysis of variance (ANOVA) with post hoc Tukey HSD was used in the statistical analysis of the data shown in panel b: *, $p < 0.1$; **, $p < 0.01$; ***, $p < 0.001$; ****, $p < 0.0001$.

4.2.3. Intracellular delivery of an antibody complex

A macromolecular construct of 580 kDa was designed to test the capabilities of the WYKYW tag. Inducing endocytosis of large protein cargoes, such as therapeutically relevant immunoglobulins at low, pharmacologically relevant concentrations, was desired. The construct contains NeutrAvidin as a connection hub, the WYKYW-containing carrier tag biotinyl-PEG-WYKYW or biotinyl-Penetratin-GG-WYKYW, a biotinylated primary immunoglobulin G, and a secondary antibody labeled with r-phycoerythrin (Figure 22a).

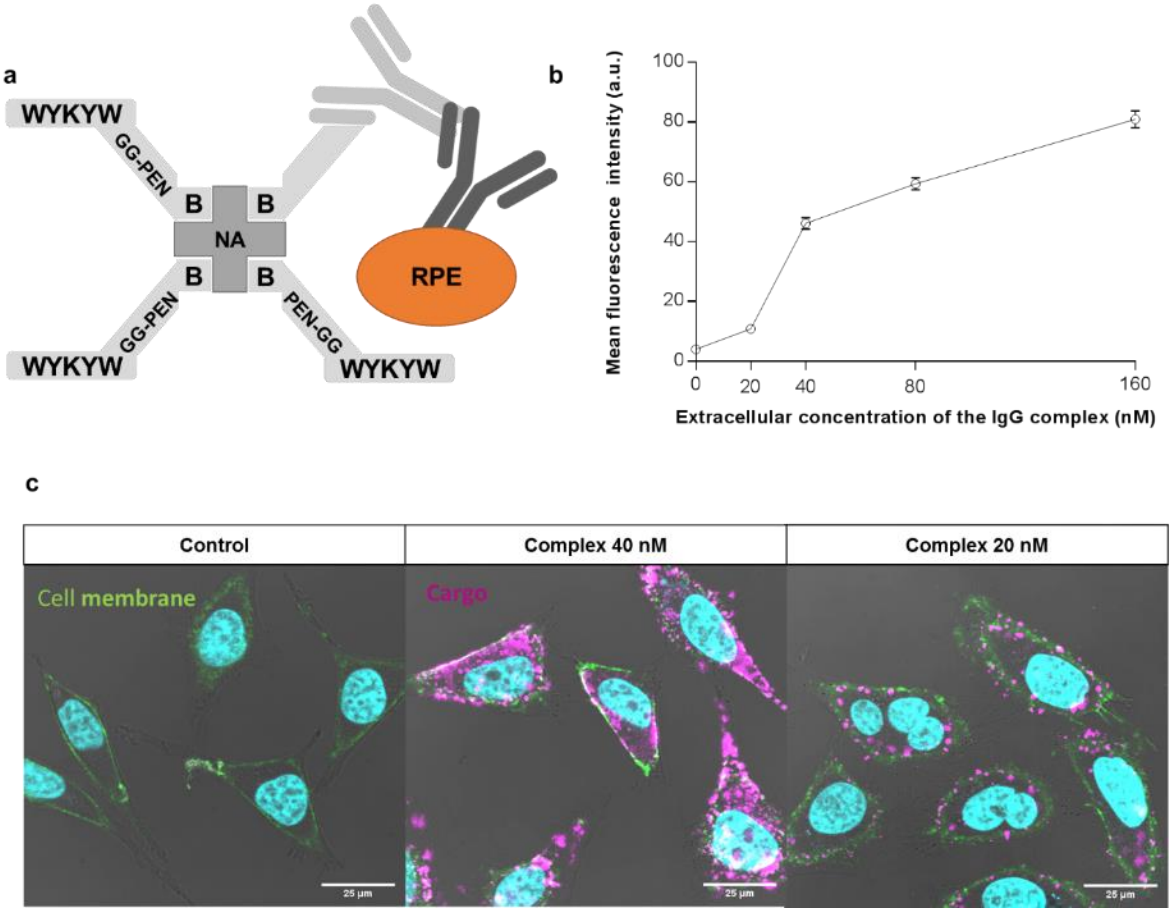

Figure 22. (**a**) Schematic representation of the bottom-up designed modular carrier–hub–antibody cargo–secondary antibody–r-phycoerythrin construct. (**b**) Artificial intelligence-aided quantitative analysis of the live CLSM images. HeLa cells were incubated for 6 hours with various concentrations of the IgG complex; at least 75 representative cells were then analyzed at each concentration. The intensity value obtained for the control sample is indicated at zero concentration. (**c**) Delivery of the IgG complex into HeLa cells at various concentrations after 3 hours. R-phycoerythrin-conjugated secondary antibody is indicated in magenta; green staining defines cell membranes (WGA-FITC). Nuclei are indicated in cyan. Control cells were treated with r-phycoerythrin-labeled secondary antibody at 160 nM for 3 hours.

To test the possible lower limit of the affinity-driven endocytic material flux, we performed the experiments close to the measured K_D for the complex (21 nM). Surface-bound fractions could not be eliminated with trypan blue quenching; therefore, the samples were subjected to thorough washing with unlabeled NA(biotinyl-Penetratin-GG-WYKYW)$_4$. The carrier-IgG complex with the biotinyl-Penetratin-GG-WYKYW conjugate was internalized over the concentration range 20 to 160 nM (Figure 22, 23).

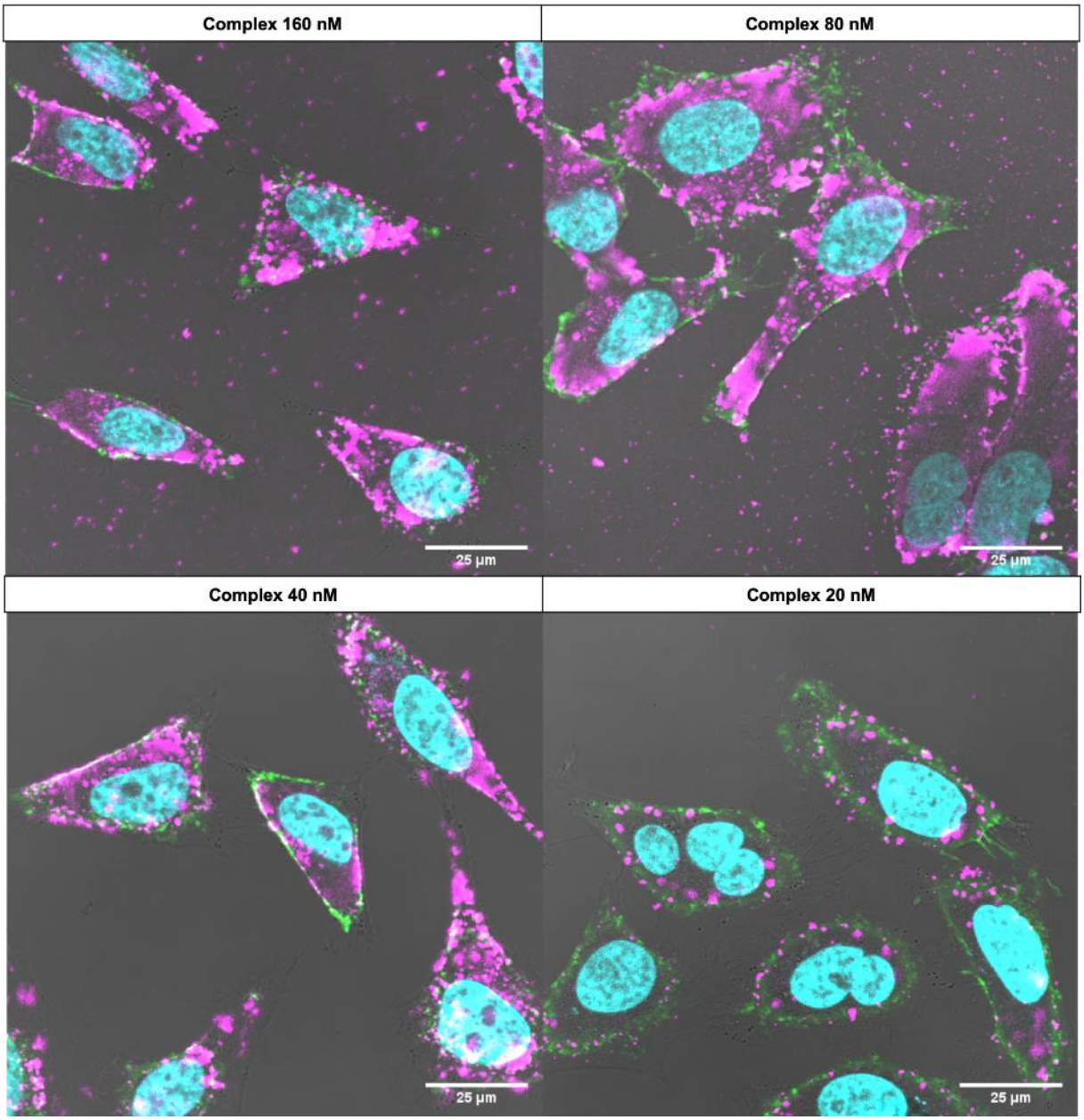

Figure 23. Enlarged CLSM images of delivery of the IgG complex into HeLa cells at different concentrations after 3 hours. R-phycoerythrin-conjugated antibody is indicated in magenta and green staining defines cell membranes (WGA-FITC). Nuclei are stained with Hoechst33342 (indicated in cyan).

During sample preparation with biotinyl-PEG-WYKYW, protein precipitation was observed, which suggests that the linker region could function as a customizable segment to stabilize the carrier–cargo complexes in solution. An important finding was that diffuse fluorescence could be observed between endosomes throughout the cytoplasm when our IgG complex was applied at concentrations above 40 nM. This can indicate the ability of the system to

escape the internalized compartments. Visual inspection suggested that the amount of internalized cargo decreased at 20 nM; therefore, artificial intelligence-aided quantitative analysis of the CLSM images was conducted (Figure 22b, 24).

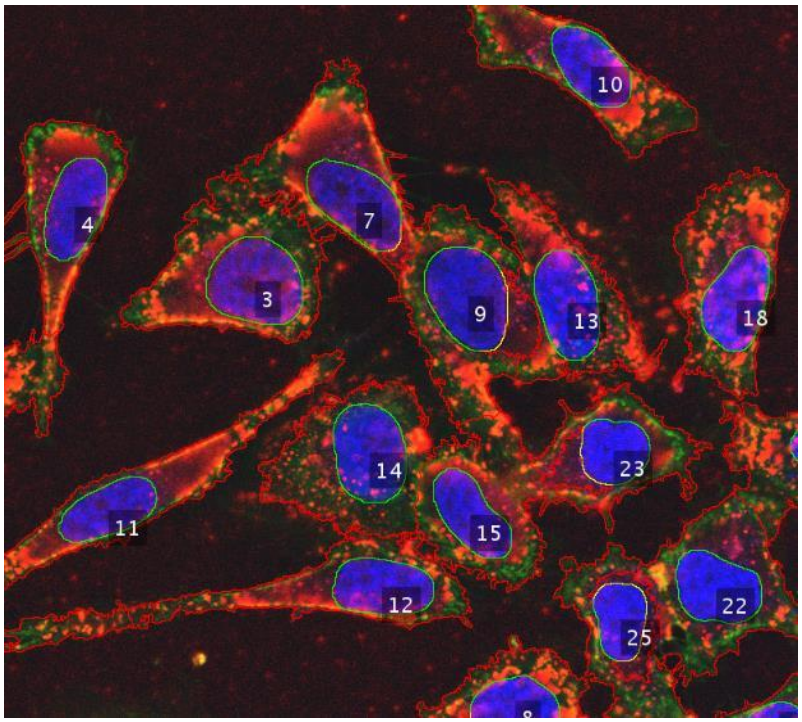

Figure 24. An example of the artificial intelligence-aided quantification of the CLSM images. HeLa cells were incubated with the IgG complex at 160 nM for 3 hours. R-phycoerythrin-conjugated antibody is indicated in red, membrane marker FITC-WGA in green. Hoechst labeled blue nuclei were identified with a deep learning-based platform, and cytoplasm was approximated with an algorithm. Red intensity values were extracted.

Results confirmed that the complex containing the WYKYW tag, which recognizes GM1, was a robust carrier agent, that triggers endocytosis and translocation of the 580 kDa cargo at extracellular concentrations corresponding to those in lower range of therapeutic protocols (ca. 100 nM). Decrease of the translocated cargo at 20 nM was confirmed by the analysis, which places the lowest performance limit close to the K_D value of the WYKYW–GM1 interaction. This can be explained by the law of mass action, and it supports the idea that the endocytosis of the cargo is driven by the GM1 affinity tag.

4.2.4. Functionality of the delivered cargoes

As r-phycoerythrin is a large, chemically sensitive protein, we considered that the intense intracellular fluorescence emission of the cargo was a telltale sign of the functional protein. To test

the possible degradation of the IgG components between the carrier and the cargo, a co-localization experiment was conducted with FITC–NeutrAvidin used in the carrier, and an Alexa Fluor 647-tagged secondary antibody in the cargo (Figure 25).

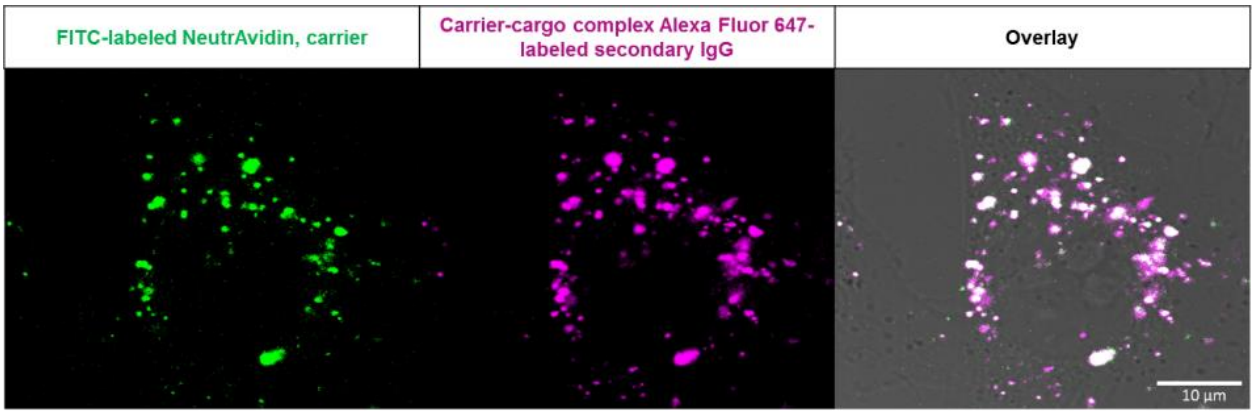

Figure 25. Internalization of the carrier–cargo complex into HeLa cells at 500 nM after 3 hours as determined by live confocal laser scanning microscopy. The FITC-labeled NeutrAvidin is indicated in green, the Alexa Fluor 647-labeled secondary IgG is indicated in magenta. Overlay of the images shows co-localization in the cell.

High spatial correlation was found between the two fluorescent signals, which supported that the molecular recognition between the primary and secondary antibody was functional. To further test the structural integrity of the primary antibody, HeLa cells were treated with a carrier–cargo complex containing only a primary anti-galectin-1 antibody attached to the carrier, and the internalized IgG component was visualized by using Atto 488-labeled galectin-1, after fixation and permeabilization of the cells. Control cells not treated with the carrier–cargo complex did not display fluorescence, while the internalized antibody bound the fluorescent galectin-1 in the treated cells, and fluorescent signal was observed. This finding suggested that the Fv region of the primary antibody was structurally intact after internalization (Figure 26).

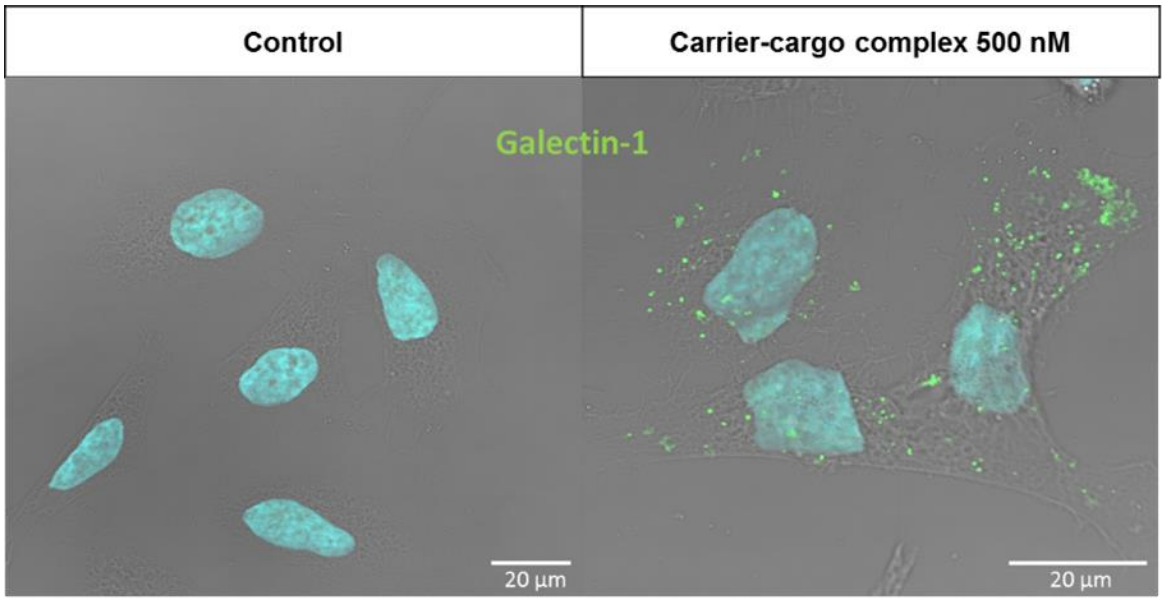

Figure 26. Internalization of the carrier–cargo complex biotinyl-Penetratin-GG-WYKYW: NeutrAvidin:Primary IgG 2c1/6 (anti-galectin-1) at 500 nM after 3 hours. After the incubation period, the cells were fixed, permeabilized, and Atto488-labeled galectin-1 (350 nM, indicated in green) was applied to visualize the internalized carrier–cargo complex. Nuclei are stained with Hoechst33342 (indicated in cyan). Control cells were incubated in culture media without the carrier–cargo complex and then treated the same way with Atto488-labeled galectin-1.

To establish a binding affinity – internalization efficiency relationship, several variants of the Biotin-Penetratin-GG-WYKYW construct was synthesized, the previously described antibody complex was prepared (Figure 22a), and their internalization efficiency was monitored with CLSM (Figure 27). HeLa cells were incubated for 1 hour with the antibody complexes at 80 nM extracellular concentrations. Substituting the tryptophan of the C-terminal with alanine significantly decreased binding. However, visual inspection showed uptake for all constructs, even with the low-binder WYKYA sequence. We carried out an AI-based quantitation with the different analogues (Figure 28). HeLa Cells were incubated with the complexes for 1 or 4 hours at an extracellular concentration of 80 nM. We could not find strong correlation between the monomer K_Ds and the internalization efficiency. The worst binder WYKYA (with a micromolar K_D) showed the lowest uptake; however, the best identified binder W^{β}YKYW did not show the highest uptake. This can happen, if the substitution made it less selective towards ganglioside GM1 and the sequence can also bind molecules inducing non-endocytosis. Surprisingly, the AYKYW construct, for which we could not fit the ITC enthalpogram, outperformed the other analogues at 80 nM after 4 hours. Our hypothesis was that above 40 nM extracellular concentration, the tryptophan

sidechains can interact significantly with aspecific protein interfaces. Above this concentration these sidechains are prone to aggregating also, therefore reducing the Trp content of the sequence can be beneficial.

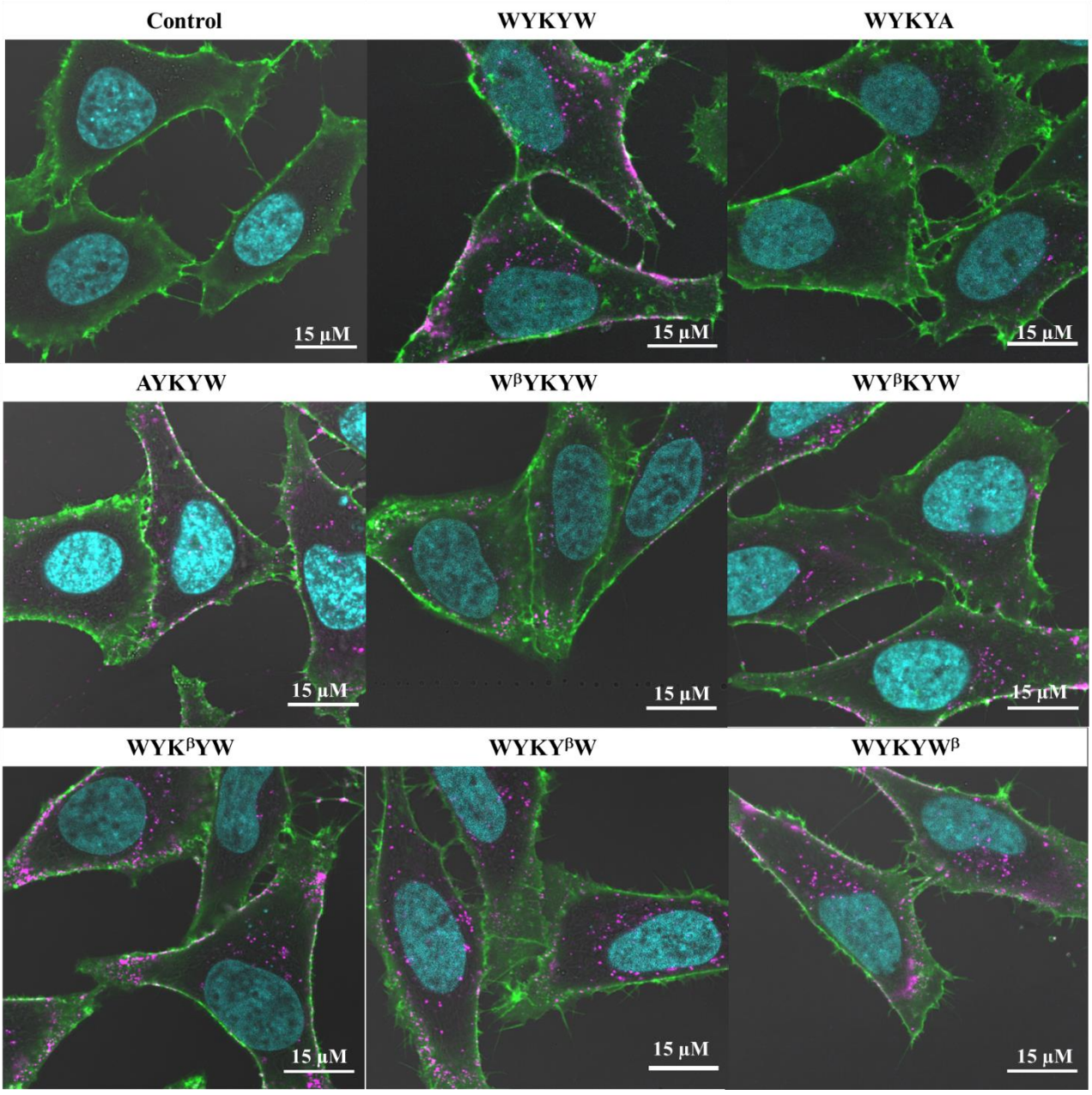

Figure 27. Delivery of the IgG complex into HeLa cells at 80 nM after 1 hour. Pictures are designated by the abbreviation of peptides examined: Biotinyl-Penetratin-GG-XXXXX, where WYKYW is the original sequence, A denotes an alanine substitution and β denotes the corresponding beta amino acid. Alexa Fluor 647-conjugated secondary antibody is indicated in magenta; green staining defines cell membranes (WGA-FITC). Nuclei are indicated in cyan. Control cells were treated with IgG complex without the ganglioside binding peptides.

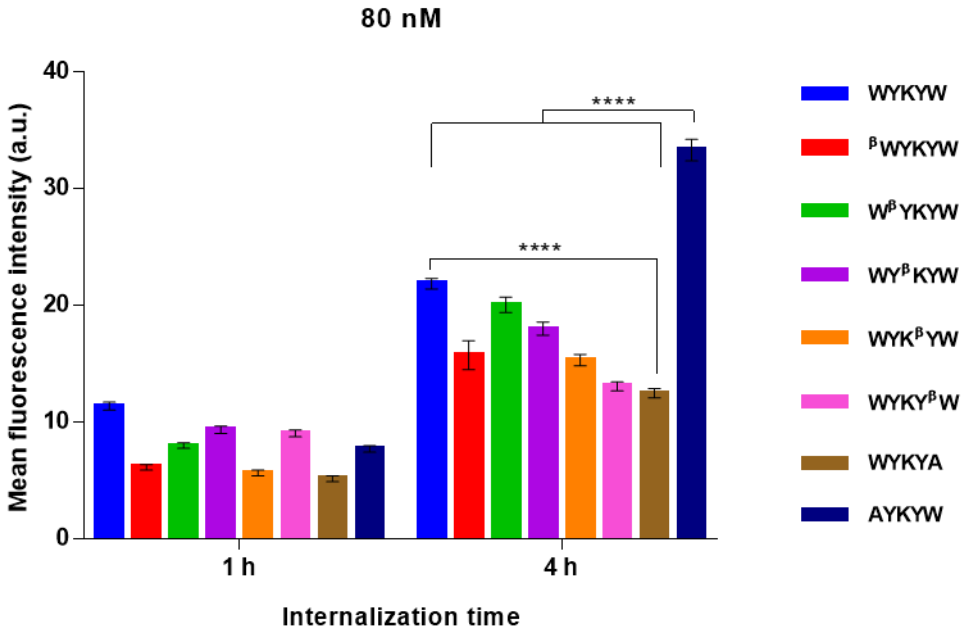

Figure 28. Quantitative analysis of the live CLSM images aided by artificial intelligence. HeLa cells were incubated for 1 or 4 hours with the IgG complexes at 80 nM; at least 150 representative cells were then analyzed at each setup. The intensity value obtained for the control sample is subtracted. Statistical analysis was performed using one-way analysis of variance (ANOVA) with post hoc Tukey HSD. ****, $p < 0.0001$.

Our next hypothesis was that even though a weak binding is achieved by a monomer Penetratin-GG-WYKYW analogue sequence, linking multiple peptides together with the NeutrAvidin protein hub and increasing the avidity can result in a binding strong enough to achieve endocytosis. To test this, we prepared the NA(biotinyl-Penetratin-WYKYA)$_4$ and the NA(biotinyl-Penetratin-WYK$^{\beta}$YW)$_4$ constructs where the K_Ds of the monomers were 1060 nM and 332 nM, respectively. ITC measurements showed that the resulting K_Ds of the multivalent constructs went down to 60.5 nM and 38 nM, respectively (Figure 29). This showed us, that even a weak binding to the ganglioside GM1 can be sufficient, if we apply our avidity-increasing method based on the avidin–biotin interaction.

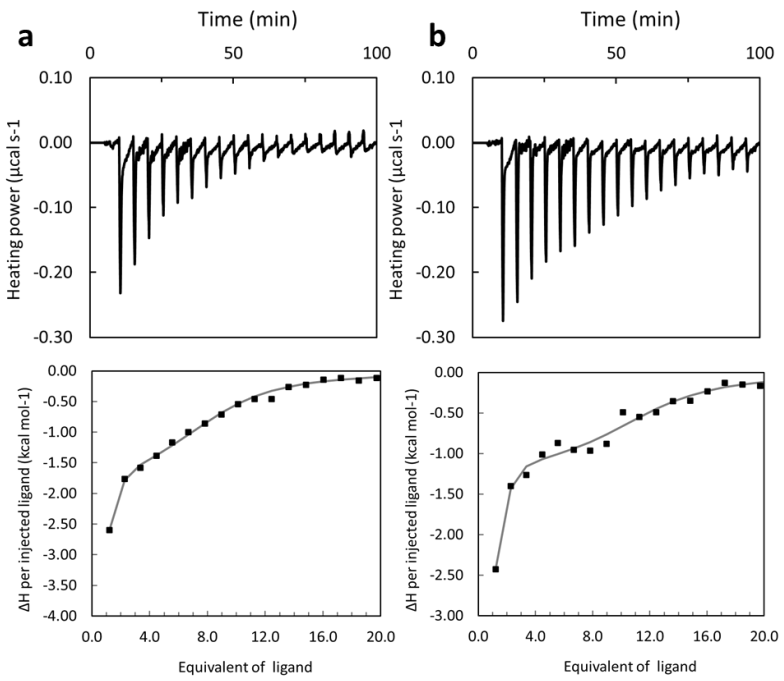

Figure 29. ITC detection of interactions of GM1 with derivatives. Enthalpograms of (**a**) NA(biotinyl-Penetratin-WYKYA)$_4$ (n_1 = 1, K_{D1} = 60.5 nM) and (**b**) NA(biotinyl-Penetratin-WYK$^{\beta}$YW)$_4$ (n=1, K_D= 38 nM). Titrations were carried out with GM1:DPC 1:5 bicelles (solid square), and nonlinear least-squares fitting was performed against the two-independent-binding-site model (solid lines).

5. Conclusions

Mammalian cells exert strict control over macromolecular traffic through the cell membrane to cellular compartments. Lipid raft-mediated/caveolar endocytosis is the most promising method for delivering cargo proteins in their functional form, as exemplified by viruses and bacterial toxins. Therefore, our concept was to steer the macromolecular cargo toward lipid raft-mediated/caveolar endocytosis and to avoid the clathrin-mediated and macropinocytosis pathways. We focused on the initial molecular recognition events that occur at endocytic membrane pits, because this facilitated both the selection of the mechanism and the effective enrichment of the low-concentration cargo at the entry point. We found that the WYKYW-tag binds the glycan moiety of the caveolar receptor GM1 with high affinity. The lack of strong interactions with GM3 and asialo-GM1 indicated selective behavior. We concluded that both the sialyl group and the terminal N-Ac-digalactoside in GM1 are essential structural features for the low-nanomolar binding. We found that alanine or D-amino acid substitution decreases the binding, while certain beta-amino acids can retain the high-affinity interaction. We observed that the membrane has an important part in the binding phenomenon, directing the peptide to its receptor.

An important feature of the WYKYW-tag is that it can effectively route the macromolecular cargo to the desired lipid raft-mediated/caveolar endocytosis entry point, and it can induce the pinch-off process even when attached to a large cargo containing IgG proteins. Based on the specific affinity-based directing effect of WYKYW, we define the term ‘endocytosis routing sequence’. Although multivalent binding of caveolar GM1 has been reported to be necessary to trigger endocytosis, we found that incorporation of a single WYKYW segment into the chain is sufficient to initiate internalization through GM1 binding.

As expected for the lipid raft-mediated/caveolar pathway, the progression of the internalized caveolae to early endosomes and later to lysosomes was absent or very slow; therefore, no colocalization with lysosomes was observed, sparing the cargo from early degradation. This may have promoted partial escape of the cargo from the endosomes, which could be observed in our experiments as diffuse intracellular fluorescence. This feature opens a path to further development of the endocytosis routing sequence presented here. Tagging the protein cargo with the large fluorescent protein r-phycoerythrin allowed us to test the functionality of the intracellular protein. The selected mechanism left the protein cargo intact, as shown by its fluorescence even

after hours of incubation. Moreover, the molecular recognition between the primary and secondary antibodies and between the primary antibody and its externally added antigen was functional indicating the absence of degradation of the carrier–cargo complex. We concluded that beta-amino acid substituted analogues can be used to achieve the translocation of the cargo when using an avidity increasing method.

Our GM1 receptor-based modular approach is a useful alternative to the currently available carriers, because the very short, easily applied, and nontoxic WYKYW-tag facilitates the advantageous lipid-raft mediated/caveolar endocytosis in a carrier-triggered manner, and it works at therapeutically relevant concentrations for cells expressing GM1. It is increasingly important to develop methods for cell- and tissue-specific targeting of cargoes. While efforts have been made to achieve specific targeting, selectivity toward cancer cells is still of great interest. The GM1-dependent endocytosis of WYKYW-tagged cargo offers selectivity for cell types that overexpress GM1, a characteristic of many tumor cells. This cell-type-dependent effect is strongly supported by the results of our experiments with HeLa and Jurkat cells, which display different amounts of GM1 on the cell surface.

6. Summary

1. We synthesized a lead molecule (peptide WYKYW) and measured its interaction with different gangliosides (GM1, asialo-GM1, GM3). We showed that the sequence had high affinity (K_D = 23.8 nM) and was specific towards ganglioside GM1. We showed that truncating the ganglioside GM1 resulted in decreased or completely abolished binding.

2. We found that fluorescent tagging in proximity of the peptide tag was detrimental to the ganglioside binding. We introduced and synthesized two linkers to lengthen the tag: a PEG-based one and a cell penetrating peptide (penetratin). We showed that both constructs retained high affinity towards ganglioside GM1.

3. We used a medicinal chemistry approach to set up a structure–activity relationship between the amino acids of the sequence and their binding efficiency. We demonstrated that every amino acid and their configuration was important in the binding. We identified several sequence analogues constructed with backbone homologation, which had comparable affinity with the parent sequence.

4. We revealed the importance of the membrane components in the binding. We measured both the tryptophan insertion into the membrane and the decreased aromatic face-to-edge interactions during the binding.

5. We showed that the peptide tag was capable of triggering endocytosis at submicromolar concentrations of a 63 kDa protein, while avoiding the lysosomal pathways.

6. We proved that the translocation was energy dependent, and that the process could be blocked with methyl-β-cyclodextrin, which showed that the endocytosis was lipid raft-mediated.

7. We demonstrated that the internalization was in correlation with the ganglioside GM1 content of the cells.

8. We carried out an in vivo titration with galectin-1, which could decrease the uptake of our complex to the base level displayed by our linker alone, strengthening the biomimetic behavior of our carrier. We confirmed this finding by observing co-localization of our complex and cholera toxin B subunit.

9. We showed that the WYKYW-tagged sequence could efficiently internalize antibody complexes (ca. 580 kDa) into human cells at low nanomolar concentrations. We observed a diffuse fluorescence throughout the cytoplasm, which we confirmed with artificial intelligence aided quantitative analysis.

10. We verified that the molecular recognition between the primary and the secondary antibodies is functional. We showed that the delivered primary antibody is structurally intact.

11. We showed that substituted sequences could internalize the IgG complex. We demonstrated that weaker binder sequences could be sufficient when increasing the avidity of the construct. We showed that decreasing the tryptophan content of the peptide tag was beneficial to the uptake of the construct.

7. Acknowledgements

I would like to express my sincere gratitude to my supervisor **Prof. Tamás Martinek** for the continuous support of my Ph.D. study and related research, for his motivation and immense knowledge. His guidance helped me during the time of research and writing of this thesis and set a great example to follow.

I owe my special thanks to **Dr. Anasztázia Hetényi** for the great amount of help with conducting and evaluating NMR and ITC measurements.

My sincere thanks also go to **Dr. Éva Monostori**, **Dr. Ágnes Czibula**, and **Dr. Enikő Szabó** in the Biological Research Centre, for always being helpful and constructive, and teaching me the ways of conducting biological research.

I would like to thank **Dr. Mária Deli** and **Dr. Péter Horváth** and their research groups for conducting the cytotoxicity experiments and supporting us with computer-aided analysis.

I owe my thanks to all my colleagues for their help and useful advice and for all the fun we have had in the last couple of years.

Finally, I would like to thank my family and friends for supporting me during my Ph.D. studies.

8. References

[1] K. Fosgerau and T. Hoffmann, *Drug Discovery Today*, **2015**, *20*, 122-128.
[2] M. Sánchez-Navarro, M. Teixidó and E. Giralt, *Nature Chemistry*, **2017**, *9*, 727.
[3] L. Pelkmans, T. Burli, M. Zerial and A. Helenius, *Cell*, **2004**, *118*, 767-780.
[4] L. Pelkmans, J. Kartenbeck and A. Helenius, *Nature Cell Biology*, **2001**, *3*, 473-483.
[5] R. Fajka-Boja, A. Blasko, F. Kovacs-Solyom, G. Szebeni, G. Toth and E. Monostori, *Cellular and Molecular Life Sciences*, **2008**, *65*, 2586-2593.
[6] R. Montesano, J. Roth, A. Robert and L. Orci, *Nature*, **1982**, *296*, 651-653.
[7] A. E. Smith and A. Helenius, *Science*, **2004**, *304*, 237-242.
[8] V. Pietiainen, V. Marjomaki, P. Upla, L. Pelkmans, A. Helenius and T. Hyypia, *Molecular Biology of the Cell*, **2004**, *15*, 4911-4925.
[9] A. L. Kiss and E. Botos, *Journal of Cellular and Molecular Medicine*, **2009**, *13*, 1228-1237.
[10] L. Pelkmans and A. Helenius, *Traffic*, **2002**, *3*, 311-320.
[11] S. Mayor, K. G. Rothberg and F. R. Maxfield, *Science*, **1994**, *264*, 1948-1951.
[12] R. R. Sprenger, R. D. Fontijn, J. Van Marle, H. Pannekoek and A. J. Horrevoets, *Biochemical Journal*, **2006**, *400*, 401-410.
[13] P. Moscariello, D. Y. W. Ng, M. Jansen, T. Weil, H. J. Luhmann and J. Hedrich, *Adv Sci (Weinh)*, **2018**, *5*, 1700897.
[14] M. Zorko and Ü. Langel, *Advanced Drug Delivery Reviews*, **2005**, *57*, 529-545.
[15] T. Matsubara, R. Otani, M. Yamashita, H. Maeno, H. Nodono and T. Sato, *Biomacromolecules*, **2017**, *18*, 355-362.
[16] M. M. Fuster and J. D. Esko, *Nature Reviews: Cancer*, **2005**, *5*, 526.
[17] U. Krengel and P. A. Bousquet, *Frontiers in Immunology*, **2014**, *5*, 325.
[18] S. K. Fischer, J. Yang, B. Anand, K. Cowan, R. Hendricks, J. Li, G. Nakamura and A. Song, *MAbs*, **2012**, *4*, 623-631.
[19] S. J. Singer and G. L. Nicolson, *Science*, **1972**, *175*, 720-731.
[20] J. F. Nagle and S. Tristram-Nagle, *Biochimica et Biophysica Acta (BBA)-Reviews on Biomembranes*, **2000**, *1469*, 159-195.
[21] D. Chapman, J. Gomez-Fernandez and F. Goni, *FEBS Letters*, **1979**, *98*, 211-223.
[22] M. Edidin, *Annual Review of Biophysics and Bioengineering*, **1974**, *3*, 179-201.
[23] R. Zwaal, P. Comfurius and L. Van Deenen, *Nature*, **1977**, *268*, 358-360.
[24] G. L. Nicolson, *Biochimica et Biophysica Acta (BBA)-Reviews on Biomembranes*, **1976**, *457*, 57-108.
[25] T. Fujiwara, K. Ritchie, H. Murakoshi, K. Jacobson and A. Kusumi, *The Journal of cell biology*, **2002**, *157*, 1071-1082.
[26] D. Branton, *Philosophical Transactions of the Royal Society of London. B, Biological Sciences*, **1971**, *261*, 133-138.
[27] M. Faini, R. Beck, F. T. Wieland and J. A. Briggs, *Trends in Cell Biology*, **2013**, *23*, 279-288.
[28] A. V. Shnyrova, P. V. Bashkirov, S. A. Akimov, T. J. Pucadyil, J. Zimmerberg, S. L. Schmid and V. A. Frolov, *Science*, **2013**, *339*, 1433-1436.
[29] D. J. López, M. Egido-Gabas, I. López-Montero, J. V. Busto, J. Casas, M. Garnier, F. Monroy, B. Larijani, F. M. Goñi and A. Alonso, *Biophysical Journal*, **2012**, *102*, 2077-2085.
[30] H. T. McMahon and J. L. Gallop, *Nature*, **2005**, *438*, 590-596.

[31] A. Diz-Muñoz, D. A. Fletcher and O. D. Weiner, *Trends in Cell Biology*, **2013**, *23*, 47-53.
[32] R. F. De Almeida, A. Fedorov and M. Prieto, *Biophysical Journal*, **2003**, *85*, 2406-2416.
[33] M. Tomishige, Y. Sako and A. Kusumi, *The Journal of cell biology*, **1998**, *142*, 989-1000.
[34] L. J. Pike, *Journal of Lipid Research*, **2006**, *47*, 1597-1598.
[35] D. A. Brown and E. London, *Journal of Biological Chemistry*, **2000**, *275*, 17221-17224.
[36] C. A. Lipinski, *Journal of Pharmacological and Toxicological Methods*, **2000**, *44*, 235-249.
[37] A. Finkelstein, *The Journal of general physiology*, **1976**, *68*, 127-135.
[38] D. Papahadjopoulos, S. Nir and S. Ohki, *Biochimica et Biophysica Acta (BBA)-Biomembranes*, **1972**, *266*, 561-583.
[39] J. N. Kew and C. H. Davies, *Ion channels: from structure to function*, Oxford University Press, USA, 2010.
[40] W. L. Duax, J. F. Griffin, D. A. Langs, G. D. Smith, P. Grochulski, V. Pletnev and V. Ivanov, *Biopolymers*, **1996**, *40*, 141-155.
[41] E. Hernando, V. Capurro, C. Cossu, M. Fiore, M. García-Valverde, V. Soto-Cerrato, R. Pérez-Tomás, O. Moran, O. Zegarra-Moran and R. Quesada, *Scientific Reports*, **2018**, *8*, 1-10.
[42] K. Ishibashi, S. Hara and S. Kondo, *Clinical and Experimental Nephrology*, **2009**, *13*, 107-117.
[43] M. Mueckler and B. Thorens, *Molecular Aspects of Medicine*, **2013**, *34*, 121-138.
[44] E. S. Schweikhard and C. M. Ziegler, *Current Topics in Membranes*, **2012**, *70*, 1-28.
[45] J. D. Young, S. Y. Yao, J. M. Baldwin, C. E. Cass and S. A. Baldwin, *Molecular Aspects of Medicine*, **2013**, *34*, 529-547.
[46] S. Mayor and R. E. Pagano, *Nature Reviews Molecular Cell Biology*, **2007**, *8*, 603-612.
[47] S. L. Schmid and L. L. Carter, *The Journal of cell biology*, **1990**, *111*, 2307-2318.
[48] R. S. Flannagan, V. Jaumouillé and S. Grinstein, *Annual Review of Pathology: Mechanisms of Disease*, **2012**, *7*, 61-98.
[49] S. A. Mousavi, L. Malerød, T. Berg and R. Kjeken, *Biochemical Journal*, **2004**, *377*, 1-16.
[50] H. T. McMahon and E. Boucrot, *Nature Reviews: Molecular Cell Biology*, **2011**, *12*, 517-533.
[51] L. H. Wang, K. G. Rothberg and R. G. Anderson, *Journal of Cell Biology*, **1993**, *123*, 1107-1117.
[52] J. A. Swanson and C. Watts, *Trends in Cell Biology*, **1995**, *5*, 424-428.
[53] Z. Liu and P. A. Roche, *Frontiers in Physiology*, **2015**, *6*, 1.
[54] R. Zeineddine and J. J. Yerbury, *Frontiers in Physiology*, **2015**, *6*, 277.
[55] A. Nanbo, M. Imai, S. Watanabe, T. Noda, K. Takahashi, G. Neumann, P. Halfmann and Y. Kawaoka, *PLoS Pathogens*, **2010**, *6*.
[56] N. Araki, M. T. Johnson and J. A. Swanson, *The Journal of cell biology*, **1996**, *135*, 1249-1260.
[57] V. Jayashankar and A. L. Edinger, *Nature Communications*, **2020**, *11*, 1121.
[58] S. Sonnino and A. Prinetti, *FEBS Letters*, **2009**, *583*, 597-606.
[59] D. Bolmatov, D. Soloviov and M. Zhernenkov, **2020**, *36*, 4887-4896.
[60] P. Liu, M. Rudick and R. G. Anderson, *Journal of Biological Chemistry*, **2002**, *277*, 41295-41298.
[61] S. Parpal, M. Karlsson, H. Thorn and P. Strålfors, *Journal of Biological Chemistry*, **2001**, *276*, 9670-9678.

[62] D. K. Sharma, J. C. Brown, A. Choudhury, T. E. Peterson, E. Holicky, D. L. Marks, R. Simari, R. G. Parton and R. E. Pagano, *Molecular Biology of the Cell*, **2004**, *15*, 3114-3122.
[63] J. E. Schnitzer, P. Oh, E. Pinney and J. Allard, *The Journal of cell biology*, **1994**, *127*, 1217-1232.
[64] J. F. Hancock, *Nature Reviews Molecular Cell Biology*, **2006**, *7*, 456-462.
[65] K. Simons and J. Gruenberg, *Trends in Cell Biology*, **2000**, *10*, 459-462.
[66] J. E. Schnitzer, D. P. McIntosh, A. M. Dvorak, J. Liu and P. Oh, *Science*, **1995**, *269*, 1435-1439.
[67] U. Örtegren, M. Karlsson, N. Blazic, M. Blomqvist, F. H. Nystrom, J. Gustavsson, P. Fredman and P. Strålfors, *European Journal of Biochemistry*, **2004**, *271*, 2028-2036.
[68] H. Ewers, W. Römer, A. E. Smith, K. Bacia, S. Dmitrieff, W. Chai, R. Mancini, J. Kartenbeck, V. Chambon and L. Berland, *Nature Cell Biology*, **2010**, *12*, 11-18.
[69] W. Römer, L. Berland, V. Chambon, K. Gaus, B. Windschiegl, D. Tenza, M. R. Aly, V. Fraisier, J.-C. Florent and D. Perrais, *Nature*, **2007**, *450*, 670-675.
[70] E. Klenk, *Hoppe-Seyler´ s Zeitschrift für physiologische Chemie*, **1942**, *273*, 76-86.
[71] J. P. Kamerling, *Comprehensive glycoscience*, Elsevier, 2007.
[72] L. Svennerholm, *Journal of Lipid Research*, **1964**, *5*, 145-155.
[73] R. Schauer, *Zoology (Jena)*, **2004**, *107*, 49-64.
[74] H. J. Maccioni, *Journal of Neurochemistry*, **2007**, *103 Suppl 1*, 81-90.
[75] T. Kolter, *ISRN Biochem*, **2012**, *2012*, 506160.
[76] F.-T. Brezicka, S. Olling, O. Nilsson, J. Bergh, J. Holmgren, S. Sörenson, F. Yngvason and L. Lindholm, *Cancer Research*, **1989**, *49*, 1300-1305.
[77] G. Marquina, H. Waki, L. E. Fernandez, K. Kon, A. Carr, O. Valiente, R. Perez and S. Ando, *Cancer Research*, **1996**, *56*, 5165-5171.
[78] K. Kaida, T. Ariga and R. K. Yu, *Glycobiology*, **2009**, *19*, 676-692.
[79] J. Inokuchi, *FEBS Letters*, **2010**, *584*, 1864-1871.
[80] K. Matsuzaki, K. Kato and K. Yanagisawa, *Biochimica et Biophysica Acta*, **2010**, *1801*, 868-877.
[81] P. Mukherjee, A. C. Faber, L. M. Shelton, R. C. Baek, T. C. Chiles and T. N. Seyfried, *Journal of Lipid Research*, **2008**, *49*, 929-938.
[82] Y. Suzuki, *Biological and Pharmaceutical Bulletin*, **2005**, *28*, 399-408.
[83] N. L. Wernick, D. J. Chinnapen, J. A. Cho and W. I. Lencer, *Toxins*, **2010**, *2*, 310-325.
[84] C. A. Day and A. K. Kenworthy, *Essays in Biochemistry*, **2015**, *57*, 135-145.
[85] M. G. Jobling, Z. Yang, W. R. Kam, W. I. Lencer and R. K. Holmes, *mBio*, **2012**, *3*.
[86] B. Mudrak and M. J. Kuehn, *Toxins*, **2010**, *2*, 1445-1470.
[87] C. Chen, Z. Fu, J. J. Kim, J. T. Barbieri and M. R. Baldwin, *Journal of Biological Chemistry*, **2009**, *284*, 26569-26577.
[88] A. R. Kroken, A. P. Karalewitz, Z. Fu, M. R. Baldwin, J. J. Kim and J. T. Barbieri, *FEBS Journal*, **2011**, *278*, 4486-4496.
[89] J. S. Lazo and E. R. Sharlow, *Annual Review of Pharmacology and Toxicology*, **2016**, *56*, 23-40.
[90] J. A. Wells and C. L. McClendon, *Nature*, **2007**, *450*, 1001-1009.
[91] M. P. H. Stumpf, T. Thorne, E. de Silva, R. Stewart, H. J. An, M. Lappe and C. Wiuf, *Proceedings of the National Academy of Sciences*, **2008**, *105*, 6959.

[92] R. Santos, O. Ursu, A. Gaulton, A. P. Bento, R. S. Donadi, C. G. Bologa, A. Karlsson, B. Al-Lazikani, A. Hersey and T. I. Oprea, *Nature reviews Drug discovery*, **2017**, *16*, 19.
[93] R. Chakrabarti, D. E. Wylie and S. M. Schuster, *Journal of Biological Chemistry*, **1989**, *264*, 15494-15500.
[94] H. Arnheiter and O. Haller, *The EMBO journal*, **1988**, *7*, 1315-1320.
[95] H. Maeda, *Bioconjugate Chemistry*, **2010**, *21*, 797-802.
[96] D. Pei and M. Buyanova, *Bioconjugate Chemistry*, **2018**, *30*, 273-283.
[97] R. M. Straubinger, N. Düzgünes and D. Papahadjopoulos, *FEBS Letters*, **1985**, *179*, 148-154.
[98] J. A. Roth, S. G. Swisher, J. A. Merritt, D. D. Lawrence, B. L. Kemp, C. H. Carrasco, A. K. El-Naggar, F. V. Fossella, B. S. Glisson and W. K. Hong, 1998.
[99] J. Lisziewicz, D. Sun, A. Lisziewicz and R. Gallo, *Gene Therapy*, **1995**, *2*, 218-222.
[100] R. K. Scheule, J. A. S. George, R. G. Bagley, J. Marshall, J. M. Kaplan, G. Y. Akita, K. X. Wang, E. R. Lee, D. J. Harris and C. Jiang, *Human Gene Therapy*, **1997**, *8*, 689-707.
[101] M. Green and P. M. Loewenstein, *Cell*, **1988**, *55*, 1179-1188.
[102] A. D. Frankel and C. O. Pabo, *Cell*, **1988**, *55*, 1189-1193.
[103] A. Joliot, C. Pernelle, H. Deagostini-Bazin and A. Prochiantz, *Proceedings of the National Academy of Sciences*, **1991**, *88*, 1864-1868.
[104] G. Lättig-Tünnemann, M. Prinz, D. Hoffmann, J. Behlke, C. Palm-Apergi, I. Morano, H. D. Herce and M. C. Cardoso, *Nature Communications*, **2011**, *2*, 1-6.
[105] Z. Qian, J. R. LaRochelle, B. Jiang, W. Lian, R. L. Hard, N. G. Selner, R. Luechapanichkul, A. M. Barrios and D. Pei, *Biochemistry*, **2014**, *53*, 4034-4046.
[106] L. D. Walensky, A. L. Kung, I. Escher, T. J. Malia, S. Barbuto, R. D. Wright, G. Wagner, G. L. Verdine and S. J. Korsmeyer, *Science*, **2004**, *305*, 1466-1470.
[107] C. Douat, C. Aisenbrey, S. Antunes, M. Decossas, O. Lambert, B. Bechinger, A. Kichler and G. Guichard, *Angewandte Chemie International Edition*, **2015**, *54*, 11133-11137.
[108] K. Saar, M. Lindgren, M. Hansen, E. Eiríksdóttir, Y. Jiang, K. Rosenthal-Aizman, M. Sassian and Ü. Langel, *Analytical Biochemistry*, **2005**, *345*, 55-65.
[109] S. El-Andaloussi, P. Järver, H. J. Johansson and U. Langel, *Biochemical Journal*, **2007**, *407*, 285-292.
[110] A. Gautam, H. Singh, A. Tyagi, K. Chaudhary, R. Kumar, P. Kapoor and G. Raghava, *Database*, **2012**, *2012*.
[111] J. W. Harbour, L. Worley, D. Ma and M. Cohen, *Archives of Ophthalmology*, **2002**, *120*, 1341-1346.
[112] E. L. Snyder, B. R. Meade, C. C. Saenz and S. F. Dowdy, *PLoS Biology*, **2004**, *2*, e36.
[113] H. Nagahara, A. M. Vocero-Akbani, E. L. Snyder, A. Ho, D. G. Latham, N. A. Lissy, M. Becker-Hapak, S. A. Ezhevsky and S. F. Dowdy, *Nature Medicine*, **1998**, *4*, 1449-1452.
[114] K. Fujimoto, R. Hosotani, Y. Miyamoto, R. Doi, T. Koshiba, A. Otaka, N. Fujii, R. D. Beauchamp and M. Imamura, *Cancer Letters*, **2000**, *159*, 151-158.
[115] K. Datta, C. Sundberg, S. A. Karumanchi and D. Mukhopadhyay, *Cancer Research*, **2001**, *61*, 1768-1775.
[116] L. Yang, T. Mashima, S. Sato, M. Mochizuki, H. Sakamoto, T. Yamori, T. Oh-hara and T. Tsuruo, *Cancer Research*, **2003**, *63*, 831-837.
[117] E. Makino, M. Sakaguchi, K. Iwatsuki and N.-h. Huh, *Journal of Molecular Medicine*, **2004**, *82*, 612-620.
[118] A. Bhoumik, L. Gangi and Z. e. Ronai, *Cancer Research*, **2004**, *64*, 8222-8230.

[119] J. J. Cronican, K. T. Beier, T. N. Davis, J.-C. Tseng, W. Li, D. B. Thompson, A. F. Shih, E. M. May, C. L. Cepko and A. L. Kung, *Chemistry & Biology*, **2011**, *18*, 833-838.
[120] D. B. Thompson, J. J. Cronican and D. R. Liu, in *Methods in Enzymology*, Elsevier, 2012, vol. 503, pp. 293-319.
[121] D. A. Rhodes and D. A. Isenberg, *Trends in Immunology*, **2017**, *38*, 916-926.
[122] J. N. Douglas, L. Gardner and M. Levin, *Journal of Clinical & Cellular Immunology*, **2013**, *4*, 134.
[123] G. Freund, A.-P. Sibler, D. Desplancq, M. Oulad-Abdelghani, M. Vigneron, J. Gannon, M. H. Van Regenmortel and E. Weiss, 2013.
[124] W.-W. Zhang, L. Li, D. Li, J. Liu, X. Li, W. Li, X. Xu, M. J. Zhang, L. A. Chandler and H. Lin, *Human Gene Therapy*, **2018**, *29*, 160-179.
[125] S. Ylä-Herttuala, *Molecular Therapy*, **2012**, *20*, 1831-1832.
[126] F. Sousa, P. Castro, P. Fonte, P. J. Kennedy, M. T. Neves-Petersen and B. Sarmento, *Expert opinion on drug delivery*, **2017**, *14*, 1163-1176.
[127] R. Aluri and M. Jayakannan, *Biomacromolecules*, **2017**, *18*, 189-200.
[128] A. Braunová, L. Kostka, L. Sivák, L. Cuchalová, Z. Hvězdová, R. Laga, S. Filippov, P. Černoch, M. Pechar and O. Janoušková, *Journal of Controlled Release*, **2017**, *245*, 41-51.
[129] M. Fathi, P. S. Zangabad, J. Barar, A. Aghanejad, H. Erfan-Niya and Y. Omidi, *International Journal of Biological Macromolecules*, **2018**, *106*, 266-276.
[130] A. Borrelli, A. L. Tornesello, M. L. Tornesello and F. M. Buonaguro, *Molecules*, **2018**, *23*, 295.
[131] A. Bolhassani, B. S. Jafarzade and G. Mardani, *Peptides*, **2017**, *87*, 50-63.
[132] M. Kristensen, D. Birch and H. Mørck Nielsen, *International Journal of Molecular Sciences*, **2016**, *17*, 185.
[133] J.-S. Liou, B. R. Liu, A. L. Martin, Y.-W. Huang, H.-J. Chiang and H.-J. Lee, *Peptides*, **2012**, *37*, 273-284.
[134] M. Akishiba, T. Takeuchi, Y. Kawaguchi, K. Sakamoto, H.-H. Yu, I. Nakase, T. Takatani-Nakase, F. Madani, A. Gräslund and S. Futaki, *Nature Chemistry*, **2017**, *9*, 751.
[135] M. Zuverink and J. T. Barbieri, *Progress in Molecular Biology and Translational Science*, **2018**, *156*, 325-354.
[136] M. Oda, Y. Terao, J. Sakurai and M. Nagahama, *Toxins*, **2015**, *7*, 5268-5275.
[137] S. Fukuta, J. L. Magnani, E. M. Twiddy, R. K. Holmes and V. Ginsburg, *Infection and Immunity*, **1988**, *56*, 1748-1753.
[138] A. Frankel, E. Tagge, J. Chandler, C. Burbage and M. Willingham, *Protein Engineering*, **1996**, *9*, 371-379.
[139] M. H. Witvliet, D. L. Burns, M. J. Brennan, J. T. Poolman and C. R. Manclark, *Infection and Immunity*, **1989**, *57*, 3324-3330.
[140] M. A. Gonzalez Porras, P. N. Durfee, A. M. Gregory, G. C. Sieck, C. J. Brinker and C. B. Mantilla, *Journal of Neuroscience Methods*, **2016**, *273*, 160-174.
[141] A. E. Smith, H. Lilie and A. Helenius, *FEBS Letters*, **2003**, *555*, 199-203.
[142] G. J. Szebeni, É. Kriston-Pál, P. Blazsó, R. L. Katona, J. Novák, E. Szabó, Á. Czibula, R. Fajka-Boja, B. Hegyi, F. Uher, L. Krenács, G. Joó and É. Monostori, *PloS One*, **2012**, *7*, e41372.
[143] K. He, G. Gkioxari, P. Dollár, R. Girshick and M. R-CNN, *IEEE, Venice, Italy*, **2017**, 2980-2988.
[144] O. Ronneberger, P. Fischer and T. Brox, *Journal*, **2015**.

[145] A. E. Carpenter, T. R. Jones, M. R. Lamprecht, C. Clarke, I. H. Kang, O. Friman, D. A. Guertin, J. H. Chang, R. A. Lindquist and J. Moffat, *Genome Biology*, **2006**, *7*, R100.
[146] P. Isola, J. Zhu, T. Zhou and A. A. Efros, 2017.
[147] S. André, C. E. P. Maljaars, K. M. Halkes, H.-J. Gabius and J. P. Kamerling, *Bioorganic & Medicinal Chemistry Letters*, **2007**, *17*, 793-798.
[148] C. E. P. Maljaars, S. André, K. M. Halkes, H.-J. Gabius and J. P. Kamerling, *Analytical Biochemistry*, **2008**, *378*, 190-196.
[149] S. André, C. J. Arnusch, I. Kuwabara, R. Russwurm, H. Kaltner, H.-J. Gabius and R. J. Pieters, *Bioorganic & Medicinal Chemistry*, **2005**, *13*, 563-573.
[150] E. Wéber, A. Hetényi, B. Váczi, É. Szolnoki, R. Fajka-Boja, V. Tubak, É. Monostori and T. A. Martinek, *ChemBioChem*, **2010**, *11*, 228-234.
[151] J. Kopitz, C. von Reitzenstein, M. Burchert, M. Cantz and H.-J. Gabius, *Journal of Biological Chemistry*, **1998**, *273*, 11205-11211.
[152] L. Cantu, M. Corti, E. Del Favero and A. Raudino, *Journal of Physics: Condensed Matter*, **2000**, *12*, A321.
[153] A. J. de Jesus and T. W. Allen, *Biochimica et Biophysica Acta (BBA) - Biomembranes*, **2013**, *1828*, 864-876.
[154] L. A. Munishkina and A. L. Fink, *Biochimica et Biophysica Acta (BBA)-Biomembranes*, **2007**, *1768*, 1862-1885.
[155] J. P. Richard, K. Melikov, E. Vives, C. Ramos, B. Verbeure, M. J. Gait, L. V. Chernomordik and B. Lebleu, *Journal of Biological Chemistry*, **2003**, *278*, 585-590.
[156] J. P. Richard, K. Melikov, H. Brooks, P. Prevot, B. Lebleu and L. V. Chernomordik, *Journal of Biological Chemistry*, **2005**, *280*, 15300-15306.
[157] P. M. Fischer, N. Z. Zhelev, S. Wang, J. E. Melville, R. Fåhraeus and D. P. Lane, *The Journal of Peptide Research*, **2000**, *55*, 163-172.
[158] S. El-Andaloussi, P. Järver, H. J. Johansson and Ü. Langel, *Biochemical Journal*, **2007**, *407*, 285-292.
[159] C. F. Brewer, *Glycoconjugate Journal*, **2002**, *19*, 459-465.
[160] J. He and L. G. Baum, *Journal of Biological Chemistry*, **2004**, *279*, 4705-4712.